



Uio • University of Oslo

# Study of the membrane protein SLC38A9 and the Rag-Ragulator complex, key effectors of mTOR Complex 1 signaling

Ange-Célia Priso Fils

Master's Degree in Molecular Biology and  
Biochemistry  
60 credits

University of Oslo  
Faculty of Mathematics and Natural sciences

April 2022



# Table of Contents

<b>Acknowledgments</b> .....	<b>vi</b>
<b>Abstract</b> .....	<b>vii</b>
<b>Abbreviations</b> .....	<b>viii</b>
<b>1 Introduction</b> .....	<b>1</b>
1.1 mTOR and cell growth.....	1
1.1.1 Introduction the mTOR complexes 1 and 2.....	1
1.1.2 Role of mTOR Complex 1 in cell metabolism .....	2
1.1.2.1 Signaling pathway upstream of mTORC1 .....	2
1.1.2.2 Signaling pathway downstream of mTORC1 .....	5
1.2 Mechanisms of mTORC1's activation at the lysosomal surface .....	6
1.2.1 Ragulator.....	7
1.2.2 Rag GTPases.....	8
1.2.3 Interactions between Raptor and the Rag GTPases .....	11
1.2.4 SLC38A9 .....	12
1.3 mTORC1 and SLC38A9 in pancreatic cancer .....	14
<b>2 Aim of the Study</b> .....	<b>16</b>
<b>3 Material and Methods</b> .....	<b>17</b>
3.1 Reconstitution of the Rag-Ragulator Complex .....	17
3.1.1 Cloning of the subunits : RagA, RagC and Ragulator .....	18
3.1.1.1 PCR, Agarose gel electrophoresis, Gel Extraction .....	18
3.1.1.2 Gibson Assembly and Transformation.....	19
3.1.1.3 Miniprep, DNA quantification and sequencing .....	20
3.1.2 Expression and growth in LOBSTR cells.....	20
3.1.3 Purification of the Rag GTPases and Ragulator constructs .....	21
3.1.3.1 Bacteria cell lysis .....	21
3.1.3.2 Affinity Chromatography of the Rag GTPases .....	22
3.1.3.3 Affinity Chromatography of Ragulator.....	23
3.1.3.4 SDS-PAGE Analysis.....	24
3.1.3.5 Size exclusion purification.....	24
3.1.4 Rag-Ragulator complex reconstitutions.....	25
3.1.4.1 Nucleotide exchange on RagA.....	26
3.1.4.2 Nucleotide exchange on RagC.....	27

3.1.4.3	Nucleotide exchange on the Rags dimer.....	27
3.1.4.4	Ultra Performance Liquid Chromatography .....	27
3.1.4.5	Reconstitution and purification of the Rags-Ragulator complexes.....	28
3.2	Reconstitution of SLC38A9 into a membrane scaffold protein nanodisc.....	29
3.2.1	Expression and purification of the membrane scaffold protein NW11 .....	29
3.2.1.1	Expression of NW11.....	29
3.2.1.2	Purification of NW11.....	30
3.2.2	Expression, Isolation and Purification of SLC38A9.....	31
3.2.2.1	Expression of SLC38A9 .....	31
3.2.2.2	Cell lysis and membrane isolation .....	31
3.2.2.3	SLC38A9 Purification.....	32
3.2.3	Reconstitution of SLC38A9 into the NW11 nanodisc.....	33
3.2.3.1	Determining the ideal lipid composition.....	33
3.2.3.2	Nanodisc reconstitution.....	34
<b>4</b>	<b>Results and Discussion .....</b>	<b>36</b>
4.1	Rag-Ragulator Complex reconstitution.....	36
4.1.1	Cloning, transformation and sequencing .....	36
4.1.2	Expression and purification of the core components.....	36
4.1.2.1	RagA.....	36
4.1.2.2	RagC.....	37
4.1.2.3	RagA – RagC dimer.....	38
4.1.2.4	Ragulator.....	39
4.1.3	RagA•GppNHp – RagC•GppNHp – Ragulator .....	41
4.1.3.1	Size exclusion purification of the GppNHp exchanged GTPases.....	42
4.1.3.2	UPLC Analysis .....	43
4.1.3.3	Reconstitution of the complex .....	44
4.1.4	RagA•GDP – RagC•GppNHp – Ragulator.....	45
4.1.4.1	Nucleotide exchange of RagA with GDP .....	45
4.1.4.2	Complex reconstitution.....	46
4.1.5	RagA•GDP – RagC•GDP – Ragulator .....	47
4.1.5.1	Nucleotide exchange of RagC with GDP.....	47
4.1.5.2	Nucleotide exchange of the Rags dimer with GDP.....	48
4.2	Reconstitution of SLC38A9 in an NW11 nanodisc .....	49
4.2.1	Cloning, transformation, and sequencing of NW11 .....	49
4.2.2	Expression and purification of NW11 .....	49

4.2.3	Expression and purification of SLC38A9.....	51
4.2.3.1	Affinity Purification.....	51
4.2.3.2	Size exclusion purification.....	52
4.2.4	Determination of the lipid composition and ratio for nanodisc assembly .....	53
4.2.4.1	Empty nanodisc reconstitution trials.....	53
4.2.4.2	Reconstitution trials of the nanodisc with SLC38A9 inside .....	54
4.2.5	Reconstitution of SLC38A9 into NW11 nanodiscs .....	55
<b>5</b>	<b>Conclusions and Future directions .....</b>	<b>56</b>
<b>6</b>	<b>References .....</b>	<b>58</b>
<b>7</b>	<b>Appendix .....</b>	<b>64</b>



# Acknowledgments

The work presented in this thesis concludes my Master's Degree in the department of Biosciences, at the Faculty of Mathematics and Natural sciences of the University of Oslo. The laboratory part was conducted externally, in Dr. David Sabatini's lab at the Whitehead Institute of the Massachusetts Institute of Technology in Cambridge, US.

First of all, I would like to thank Dr. Kacper Rogala, my research supervisor at the Whitehead, for believing in me and giving me the wonderful opportunity to perform this work in Dr. David Sabatini's lab. I thank him for all his guidance and support that have been of great importance in the conduction of these research projects and throughout my master studies. I would also like to thank my labmates from the Sabatini lab, for all the laughs and scientific inputs that made my time there even more special.

I also thank Dr. Hans-Petter Hersleth, my internal supervisor for his help when writing this thesis and all his valuable input.

Secondly a big thanks to Dr. Alexandre Corthay and all his lab members at Rikshospitalet, where I also performed some research, for all their help and support. I am especially grateful to Inger for the emotional support and for being an amazing ear in the darkest times. Thank you, Debbie and Brian for your friendship and for all the laughs. A special thanks to Asha, who has proven to be more of a sister than a friend throughout this important time of my life.

Last but not least, I would like to thank my amazing friends and family whose support has been more valuable than I could describe, thank you Max, Theo, and Louis for believing in me and always being there when I needed you. Finally, a special thanks to my boyfriend Diallo for all the love and happiness that helped throughout the completion of this thesis.

# Abstract

Located downstream of nutrients and growth factors, the mechanistic target of Rapamycin Complex 1 (mTORC1) is a protein kinase that coordinates cell growth with environmental conditions, promoting cell growth processes like protein and lipid synthesis in response to feeding. The activation of mTORC1 in response to amino acid levels occurs at the lysosomal surface and is controlled by a heterodimeric complex of Rag GTPases, tethered to the lysosomal membrane through its interaction with the Ragulator Complex. The membrane protein SLC38A9 senses intralysosomal amino acids levels, and transports essential amino acids to the cytosol, triggering a nucleotide switch that activates the Rag GTPases complex, and enables it to recruit mTORC1 at the lysosomal surface where it is activated by another small GTPase called Rheb.

Being at the center of cell growth, mTORC1 signaling is often mutated in cancer. Pancreatic cancer cells for example, tend to use protein scavenging as a food source, which requires the action of SCL38A9.

This thesis research aims to study the conformational changes induced by the nucleotide's switches within the Rag GTPases heterodimer at the structural level. In addition to this it focuses on the potential of SLC38A9 as a potential drug target for pancreatic cancer patients. Its reconstitution into a membrane scaffold protein nanodisc for structural studies sets the foundations for further structural biology centered drug screening experiments targeting SLC38A9. Similarly, the reconstitution of the Ragulator-Rag GTPases in different nucleotide-binding states will later enable to image them using Cryo-Electron microscopy, gaining more insight on the conformational changes induced by GTP and GDP binding within the heterodimer.

# Abbreviations

mTOR : mechanistic (previously mammalian) target of Rapamycin

mTORC1 : mechanistic target of Rapamycin Complex 1

mTORC2 : mechanistic target of Rapamycin Complex 2

SLC38A9 : Sodium-coupled neutral amino-acid transporter 9

GATOR 1 : Gap Activity TOWards Rags complex 1

GATOR 2 : Gap Activity TOWards Rags complex 2

FLCN : Folliculin

FNIP2 : Folliculin interacting protein 2

OD<sub>600</sub> : Optical density at 600 nm

SDS-PAGE : sodium dodecyl sulfate polyacrylamide gel electrophoresis

SEC : Size exclusion chromatography (also referred as Gel filtration)

SREBPs : Sterol regulatory element binding proteins

FKBP12 : 12-kDa FK506-binding protein

Rag GTPases : Rag guanosine triphosphatases

GEF : Guanine-nucleotide exchange factor

TSCC : Tuberculosis Sclerosis Protein Complex

HRV3C : Human Rhinovirus 3C protease

GST : Glutathione S-transferase

PDAC : Pancreatic ductal adenocarcinoma

EDTA: Ethylenediamine tetraacetic acid

MW: Molecular weight

w/v : Weight/Volume

CRD : C-terminal roadblock domain

NBD : Nucleotide-binding domain

UPLC : Ultra Performance Liquid Chromatography

MSP : Membrane scaffold Protein

GAP : GTPase activating protein

CV : Column volume



# 1 Introduction

## 1.1 mTOR and cell growth

The mechanistic target of Rapamycin also called mTOR is a serine/threonine Phosphoinositide 3-kinase (PI3K) related protein kinase that is part of a major nutrient-sensitive signaling network, also known as the mTOR pathway. This signaling pathway is involved in many cellular processes such as protein synthesis, lipid synthesis and autophagy, thus playing a key role in cell growth regulation (1). This protein kinase is targeted and inhibited by Rapamycin, a small molecule isolated from bacteria that possesses immunosuppressive and anti-tumor properties. Rapamycin forms a complex with the peptidyl-prolyl-isomerase FKBP12 that directly binds the FKBP-rapamycin-binding (FRB) domain of mTOR, narrowing its catalytic cleft, thus preventing substrate binding to the kinase active site, and resulting in the inhibition of cell growth and proliferation (2)(3) (Figure 1).

### 1.1.1 Introduction the mTOR complexes 1 and 2

The kinase mTOR is the catalytic subunit of two protein complexes respectively called mTOR complex 1 and mTOR complex 2 thereafter referred as mTORC1 and mTORC2 (4). mTORC1 possesses 3 main components : mTOR responsible for its catalytic activity, Raptor a regulatory protein responsible for substrate recruitment with a key role in the subcellular localization of mTORC1 (5), and finally mLST8 that stabilizes the kinase activation loop. In addition to the 3 components listed above, mTORC1 contains two inhibitory subunits : DEPTOR and PRAS40 (6)

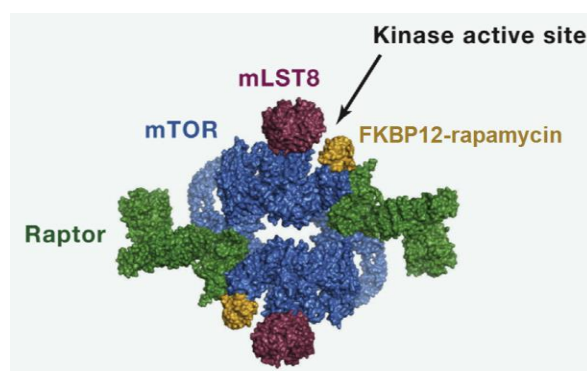


**Figure 1** : 3D structure of mTORC1 bound to FKBP12-Rapamycin.

This figure shows mTORC1's 3 core components, mTOR, the catalytic subunit of the complex ; Raptor responsible for its subcellular localization and mLST8, regulator of the kinase activation. Each of these molecules are present in double. The FKBP12-Rapamycin complex is shown in yellow. Only the two regulatory subunits PRAS40 and DEPTOR are missing in this structure). (1)

The second complex, mTORC2 also possesses mTOR, mLST8 and DEPTOR, though Raptor is there replaced by another protein of similar function : Rictor, also called Rapamycin insensitive companion. The protein complex mTORC2 also contains a regulatory subunit called mSin1. Unlike mTORC1, mTORC2 does not seem to be inhibited by rapamycin. It controls cell proliferation and survival mainly through the activating phosphorylation of Akt, an important molecule of the insulin/PI3K signaling pathway (7).

## 1.1.2 Role of mTOR Complex 1 in cell metabolism

### 1.1.2.1 Signaling pathway upstream of mTORC1

To achieve growth, cells need to promote anabolic processes such as protein and lipid synthesis, producing macromolecules through conversion of nutrients and energy, while inhibiting catabolic pathways. Located downstream of several growth controlling signals (Figure 2A and 3), mTORC1 plays a key role in controlling the balance between anabolism and catabolism in response to environmental conditions (Figure 2B) and promotes cell growth in response to growth factors, oxygen and energy levels, as well as amino acid levels (8).

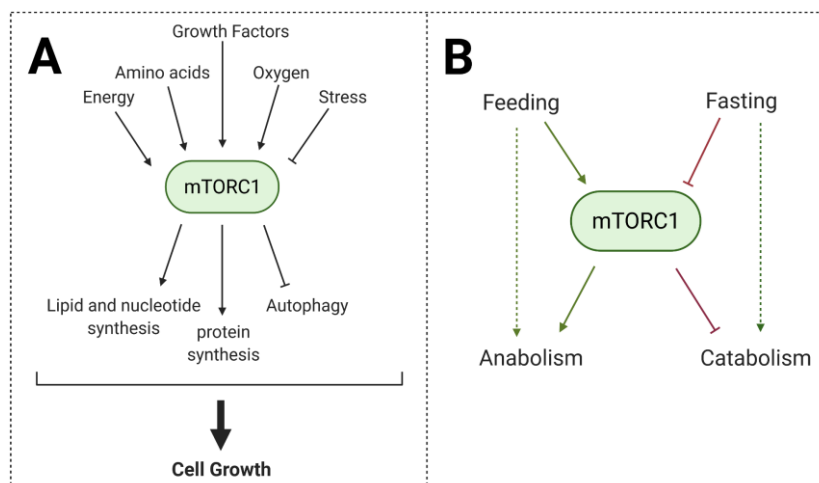


**Figure 2** : mTORC1 metabolism in response to environmental conditions. (A) Growth promoting signals such as growth factors, amino acids, and high levels of energy or oxygen , activate mTORC1

that itself activates protein and lipid synthesis, and inhibits autophagy, resulting in cell growth. (B) mTORC1 is activated in response to feeding and inhibited in response to fasting, controlling the balance between anabolism and catabolism (Figure adapted from(1)).

Growth factors influence mTORC1's activity through signaling cascades resulting in the inhibition of the Tuberous Sclerosis Protein Complex, thereafter called TSCC (Figure 3). The GAP (GTPase activating protein) activity of the TSC2 subunit of this heterotrimeric complex, that consists of the 3 subunits Tuberous Sclerosis Complex 1, 2 and 17 respectively (TSC1, TSC2 and TSC17), enables it to inhibit the small GTPase Rheb, key activator of mTORC1, through hydrolysis of its GTP nucleotide into GDP, shifting the GTPase to an inactive state (9).

The action of the TSC complex limits cell growth in response to poor-growth conditions and increases it in the presence of growth factors through the small GTPase Rheb, located downstream of growth factors and TSCC (Figure 3). In its GTP-bound active form, Rheb binds and activates mTORC1 by inducing a conformational change resulting in the stimulation of its kinase activity (6).

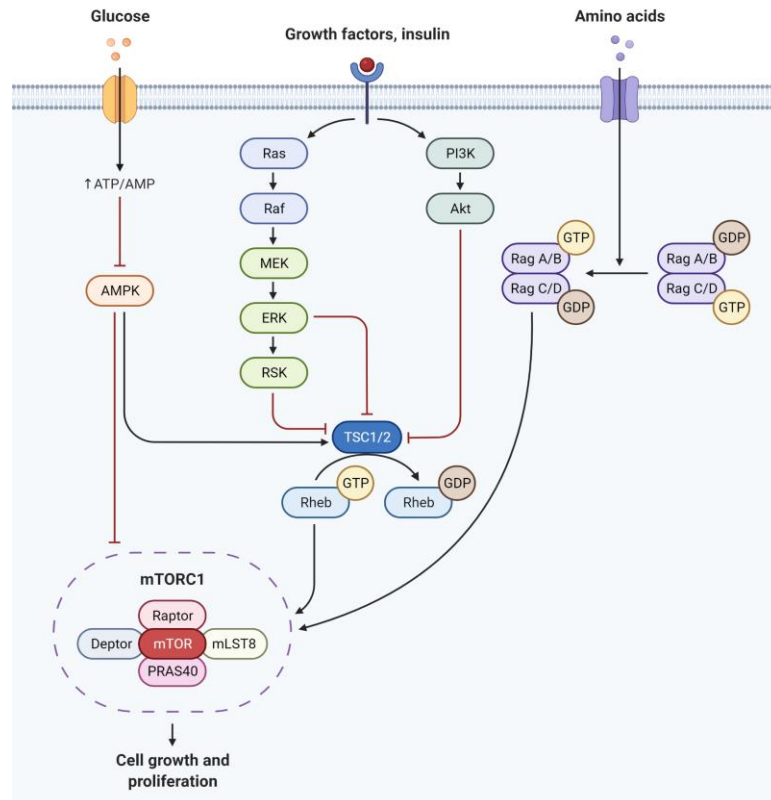


Figure 3: Upstream signaling of mTORC1 in response growth promoting signals such as growth factors, glucose and amino acids, each triggering a signaling response resulting in the regulation of mTORC1's activity (Figure adapted from Biorender).

On the other hand, low ATP levels, low energy and DNA damage, all incompatible with cell growth, also trigger an mTORC1 response. Low glucose levels and stress signals result in the activation of AMPK (AMP-dependent protein kinase), an important metabolic regulator that inhibits mTORC1 both directly, through the phosphorylation of Raptor and indirectly through the activating phosphorylation of TSC2 (Figure 3) which as mentioned above inhibits Rheb and thus mTORC1 (10,11).

mTORC1's inhibition in such conditions can also be achieved in an AMPK-independent mechanism through the inhibition of the Rag GTPases complex which plays a key role in its activation. This enables AMPK lacking cells to inhibit mTORC1 when glucose levels are low. Other conditions such as hypoxia and DNA-damage are also able to inhibit mTORC1 through AMPK dependent and independent mechanisms, very often involving TSCC (12,13).

mTORC1 is also activated in response to the increase of amino acids levels. The mechanisms, that will be discussed in detail further down, involve the Rag GTPases heterodimer of RagA or Rag B with RagC or Rag D. The presence of amino acids enables the Rag GTPases to move from an inactive state with RagA/B bound to GDP and RagC/D bound to GTP, to an active state with RagA/B bound to GTP and RagC/D bound to GDP (Figure 3), resulting in mTORC1's recruitment and activation at the lysosomal surface (14).

The GATOR1 and GATOR2 complexes (Gap Activity TOWards Rags complex 1 and 2), controlled by sestrins, are also involved in mTORC1 activation by amino acids. GATOR1 has a GTPase-activating protein activity on RagA, catalyzing the hydrolysis of its GTP bound nucleotide and thus shifting the Rags to an inactive state. GATOR2 is a GATOR1 inhibitor. During amino acid starvation, Sestrins are bound to GATOR2, blocking its inhibiting effect on GATOR1, thus keeping the Rag GTPases in an inactive state. While on the opposite, amino acid sufficiency triggers the dissociation of sestrins from GATOR2, enabling it to inhibit GATOR1 and shift the GTPases to their active state in which mTORC1's activation occurs (15). In addition to this, Arginine, a non essential amino acid plays a role in mTORC1 activation through several pathways, one of which targets TSCC-Rheb signaling, while others target the Rag GTPases complex (16,17).

### 1.1.2.2 Signaling pathway downstream of mTORC1

mTORC1 is located in the upstream signaling pathway of several transcription factors and key effectors of metabolic processes involved in cell growth such as protein, nucleotide and lipid synthesis, or autophagy inhibition (Figure 4) (8). mTORC1 initiates protein synthesis through the activating phosphorylation of S6K1 and the inhibiting phosphorylation of 4EBP1 (4E-binding protein 1, 4E is a eukaryotic translation initiation factor), both involved in the assembly of the eukaryotic initiation factor 4F (eIF4F), involved in the initiation of mRNA translation (18)(19)

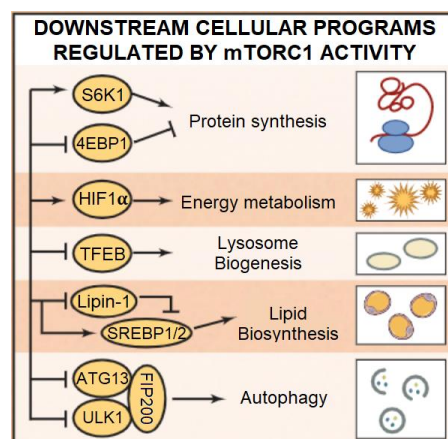


Figure 4 : Cell growth driving signaling pathways downstream of mTORC1. mTORC1 targets many proteins involved in cell growth processes such as protein synthesis, lipid synthesis, energy metabolism, lysosome biogenesis or autophagy. (20)

De novo lipid synthesis is also promoted by mTORC1 through the activation of sterol regulatory element binding proteins (SREBPs), transcription factors that control the expression of enzymes necessary for sterols and phospholipids synthesis. It also does so through the inhibition of Lipin-1, an important SREBPs inhibitor (Figure 4) (21).

In order to provide the necessary energy for the cell to achieve all these processes, mTORC1 stimulates the translation of HIF1 $\alpha$  (Hypoxia inducible factor-1 alpha), initiating a shift in glucose metabolism from oxidative phosphorylation to glycolysis enabling the cell to incorporate nutrients in its metabolism more efficiently (22). At last, mTORC1 inhibits autophagy through phosphorylation of ULK1 (Unc-51 like kinase 1, an autophagy activating kinase), a key component of the ULK1-complex, formed with ATG13 (Autophagy related 13) and FIP200 (Figure 4) involved in autophagosome formation (23).

## 1.2 Mechanisms of mTORC1's activation at the lysosomal surface

The activity of mTORC1 is mainly regulated by nutrients. The focus here is on the mechanisms of mTORC1's activation at the lysosomal surface, in response to intralysosomal amino-acid levels.

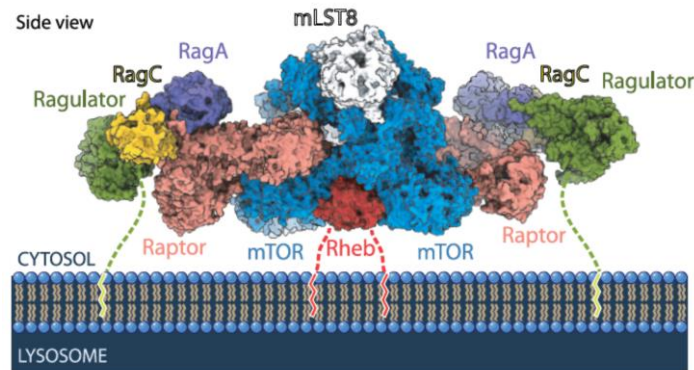


*Figure 5 : Structural side view of the docking and activation of mTOR Complex 1 at the lysosomal surface. mTORC1 is recruited to the lysosomal surface when Raptor binds the GTPases heterodimer RagA-RagC, tethered to the lysosomal membrane through its association with the Ragulator complex. (Appendix 1)*

This mechanism relies on the lysosomal membrane protein SLC38A9 (Sodium-coupled neutral amino-acid transporter 9) that is an amino acid sensor and transporter, and on the heterodimeric complex of small GTPases RagA or RagB bound to RagC or RagD, anchored to the lysosomal membrane through its interaction with the pentameric complex Ragulator (Figure 5) (24,25)

GTPases are able to change their conformation and activate or deactivate themselves by hydrolysing Guanosine Triphosphate nucleotides. The presence of amino acids inside lysosomes sensed by SLC38A9, triggers a nucleotide switch on Rag GTPases complex, shifting it from an inactive state (RagA/B bound to GDP and RagC/D bound to GTP) to an active state with RagA/B bound to GTP and RagC/D to GDP. The conformational change induced, allows Raptor to bind to the complex and dock itself in between the Rag GTPases heterodimer (Appendix 1), thus recruiting mTORC1 to the lysosomal surface where it can be activated by Rheb when growth factors are present (Figure 5 and Figure 3) (26).

Thus, SLC38A9, Rags and Ragulator all have an important role to play in mTORC1's activation at the lysosomal surface in response to amino acid levels.

## 1.2.1 Ragulator

The Ragulator complex acts as a scaffold tethering the Rag GTPases complex to the lysosomal membrane. This protein complex consists of 5 subunits : p18 (Lamtor1), p14 (Lamtor2), MP1 (Lamtor3), c7orf59 (Lamtor4/p10) and finally HBXIP (Lamtor5). p14 and MP1, are in close interactions and form a heterodimer within the complex, so do c7orf59 and HBXIP. They are packed side by side and wrapped around by p18 (Figure 6), which interacts with p14, MP1, c7orf59 and HBXIP through both hydrophilic and hydrophobic interactions, making itself essential for complex assembly (27).

The p18 subunit plays a key role in Ragulator's structure and function. In addition to its role in assembling and maintaining the complex with MP1-p14 and c7orf59-HBXIP heterodimers, p18 is also responsible for anchoring the Ragulator complex to the lysosomal membrane. Its N-terminal region is not involved in the complex assembly but contains lipid enriched sites that underwent palmitoylation and myristoylation, post-translational modifications during which saturated fatty acids are attached to single amino-acid residues (28,29). These lipid enriched regions enable p18 to interact with the lipid rafts present in the lysosomal membrane, thus tethering the whole Ragulator complex, the Rag GTPases and later mTORC1 to the lysosomal membrane. (30)

The three subunits p18, p14 and MP1 interact with the Rag GTPases heterodimer, making Ragulator essential for localizing the Rag GTPases heterodimer at the lysosomal surface. It is also known, in the presence of amino acids, to act as a Guanine nucleotide exchange factor (GEF) on RagA/B, favoring the release of its bound GDP nucleotide, thus enabling it to bind GTP and become active (31). Finally, Ragulator is also in complex with a v-ATPase at the lysosomal surface, also required for amino acids to activate mTORC1 and believed to have a role in efflux of amino acids outside lysosomes. (32)

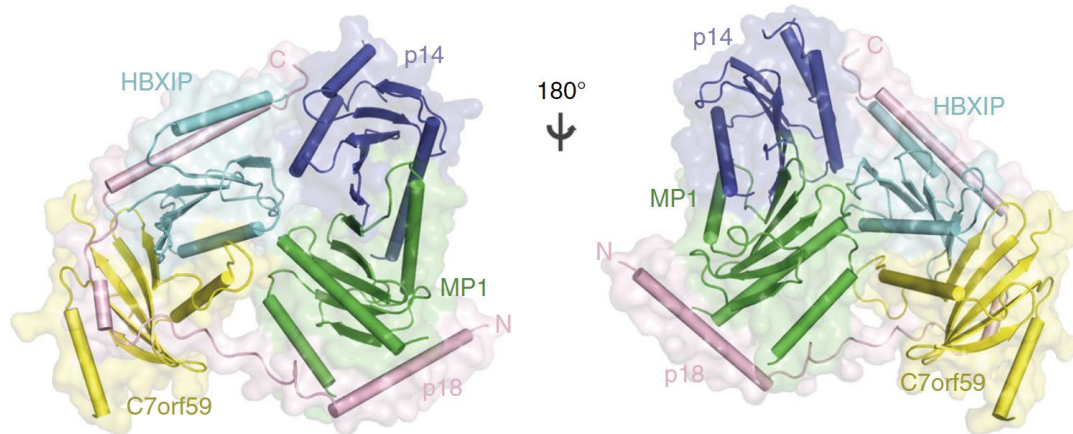


Figure 6: Structure of the Ragulator complex showing its 5 components : p18, p14, MP1, c7orf59 and HBXIP. p18 wraps around the two heterodimers formed by p14 and MP1, and c7orf59 and HBXIP respectively. (28)

## 1.2.2 Rag GTPases

The activation of mTORC1 at the lysosomal surface happens in two steps, each controlled by a different GTPase system : Rags control translocation of mTORC1 and Rheb activates its kinase activity in the presence of growth factors (33). They belong to the superfamily of Ras GTPases: GTP binding enzymes, that are able to switch between active and inactive states by hydrolyzing GTP nucleotides (34). They catalyze a large range of reactions, thus playing a key role in regulating a variety of cellular processes, such as cell-cycle progression, cell proliferation, gene expression, cytoskeletal reorganization, cell shape and polarity (35). They act as molecular switches, controlled and regulated by guanine nucleotide exchange factors (GEFs) that enable the dissociation of the GDP bound nucleotide from the GTPase, enabling it to rebind GTP and shift to its active state and GTPase activating proteins (GAPs) that stimulate the hydrolysis of these GTP nucleotides, shifting the GTPase to an inactive state (Figure 7). (36)

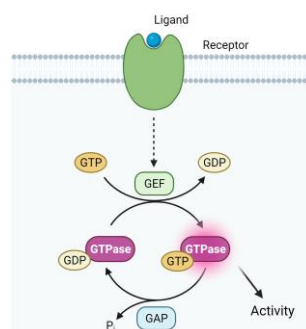


Figure 7 : GTPase activating protein (GAP) and Guanosine Exchange Factors (GEF) activities in response to

ligand-receptor signaling. The GAP activity catalyzes the hydrolysis of GTPase-bound GTP nucleotides into GDP, shifting the GTPase to an inactive state. The GEF activity on the other hand, releases the GDP nucleotides bound to the GTPase, enabling it to rebind GTP and become active. (Figure made in Biorender)

Anchored to the lysosomal surface through its interaction with Ragulator, the Rag GTPases, responsible for the translocation of mTORC1 to the lysosomal surface, are an obligate heterodimer. They form a functional unit that can bind two guanine nucleotides (as each Rag binds one guanine nucleotide). Each of them possesses a C-terminal roadblock domain (CRD), that interacts with one another and is responsible for the heterodimer's formation, and a N-terminal GTPase domain, responsible for nucleotide-binding (NBD, also called G domain) (37). The binding of the heterodimer with Ragulator relies on the interaction of their CRD with p18, p14 and MP1, enabling p18 to wrap around the three blocks of heterodimers : MP1-p14, c7orf59-HBXIP and RagA/B-RagC/D (38) (Figure 8).

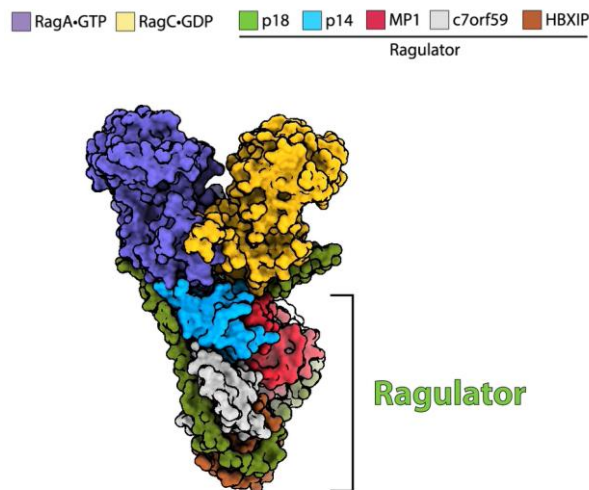


Figure 8: Structure of the Rag-Ragulator complex. The assembly relies on the interactions between the GTPases heterodimer of RagA and RagC and p14, MP1 and p18. (Figure based on Appendix 1)

The key to the heterodimer's switch between active and inactive state is the intercommunication between the two Rag GTPases subunits. GTP nucleotide-binding is highly stabilized by Mg<sup>2+</sup> ions present in the nucleotide-binding pocket of the Rags, which results in a stronger affinity of Rags with GTP than with GDP (39). The Rags dimer is stable in two nucleotide-binding states : RagA•GTP–RagC•GDP and RagA•GDP–RagC•GTP, while the two other states RagA•GDP–RagC•GDP and RagA•GTP–RagC•GTP are unstable and thus transient (40).

The functionally active nucleotide-binding state, with RagA bound to GTP and RagC bound to GDP is maintained by a key hydrogen bond between one single residue in the NBD of RagA or C and another single residue in the CRD of the opposite Rag GTPase (41).

The NBD is a network of secondary structures called switches, that experience conformational changes based on the hydrolysis or exchange of GTP and GDP nucleotides (42). The binding of GTP to one of the Rag GTPases induces a conformational change that prevents its dissociation from the NBD. Moreover, it prevents the other Rag from binding GTP (GTP binding on RagA prevents RagC to bind GTP and inversely), and stimulates the hydrolysis of the second GTP, in the case that the second Rag would indeed bind GTP, thus making RagA•GTP–RagC•GTP a highly transient state extremely unstable in nature (Figure 9) (40,43)

The activity of the Rag GTPases is not only regulated by Ragulator but also by other protein complexes such as GATOR1, acting downstream of GATOR2 and exhibiting a GAP activity towards RagA ; and FLCN-FNIP2 (folliculin in complex with the folliculin-interacting protein 2) that also exhibits a GAP activity but towards RagC, stimulating the hydrolysis of its GTP-bound nucleotide (44)

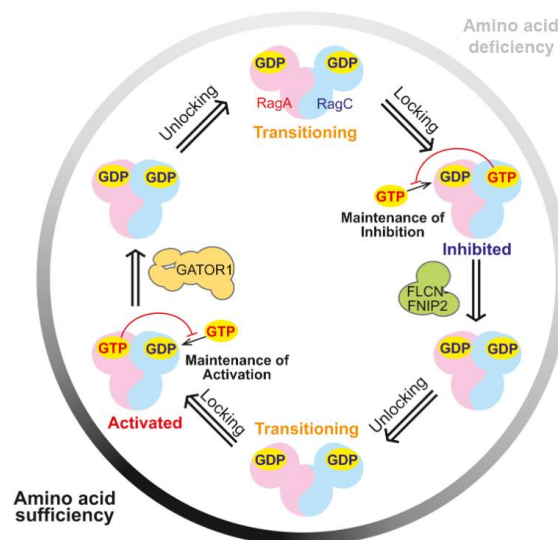


Figure 9: Activation and inactivation of the Rag GTPases based on amino acid levels. The interdomain communication between the Rag GTPases prevents both Rags from binding GTP simultaneously. Thus the action of GATOR1, hydrolysing RagA's GTP results in the inhibition of the Rags, while the action of FLCN-FNIP2, hydrolysing RagC's GTP spontaneously pushes the dimer towards its active state. (40)

Each of them plays a role in “shifting” the Rags between inactive and active states in response to amino acid levels (Figure 9). It has been shown that RagA’s exchange of GDP to

GTP occurs spontaneously (44). Thus, the hydrolysis of RagC's GTP into GDP automatically results in RagA binding a new GTP. The action of the FLCN-FNIP2 complex then converts the Rag GTPases into their active state by converting RagC•GTP into RagC•GDP, while the action of GATOR1 converts the heterodimer into its inactive state through hydrolysis of RagA•GTP into RagA•GDP (Figure 9) (45,46).

### 1.2.3 Interactions between Raptor and the Rag GTPases

mTORC1's recruitment at the lysosomal surface relies on the direct interaction of Raptor with the Rag GTPases heterodimer, which occurs in the RagA•GTP–RagC•GDP conformation, at the N-terminal nucleotide-binding domains of the GTPases. Raptor is thus the key mediator to the interaction between mTORC1 and the Rag GTPases (47)

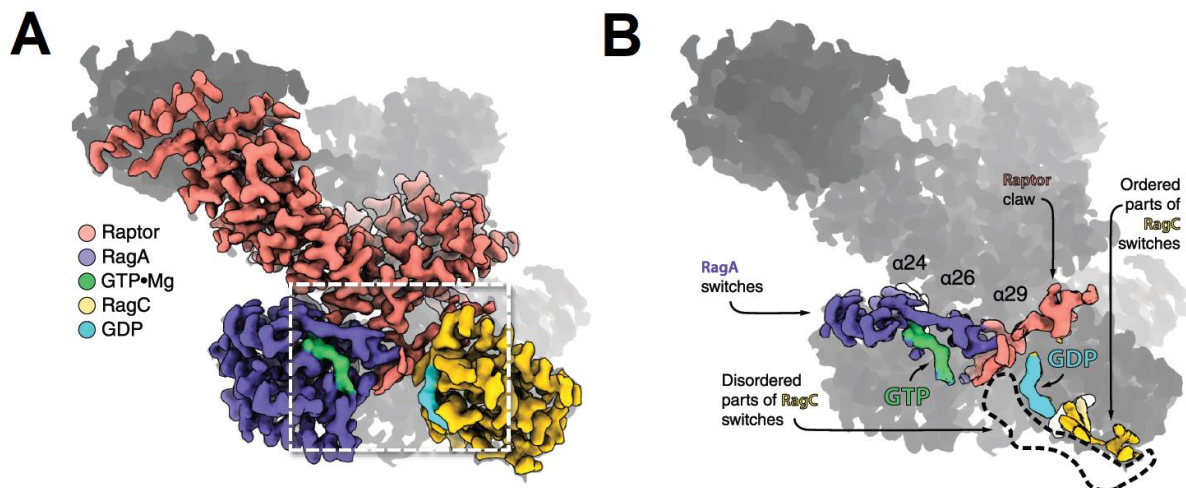


Figure 10: Interactions of Raptor with the Rag GTPases heterodimer. Raptor interacts very closely with the nucleotide-binding domains of both RagA and RagC, at several residue positions. (Appendix 1)

As mentioned previously, the GTPase domain contains secondary structures that act as switches and change conformation based on the GTPase's nucleotide-binding state. Raptor interacts with the switch I region of RagA's GTPase domain through three  $\alpha$ helices :  $\alpha 24$ ,  $\alpha 26$  and  $\alpha 29$  of its  $\alpha$ -solenoid section (Appendix 1) (Figure10). This interaction only occurs when RagA is bound to GTP, as GDP binding is thought to trigger a rearrangement in the switch I region of RagA, thus compromising its interaction with Raptor (37,48). This enables Raptor to detect RagA's nucleotide-binding state.

Nevertheless, how Raptor detects the one of RagC originally appeared to be more complex, as the  $\alpha$ -solenoid section that interacts with RagA's switches is located further away from RagC's nucleotide-binding pocket (Appendix 1). A section of Raptor, identified as the N-terminus Raptor claw, enters the space between the GTPases where it interacts with the NBD of RagC, detecting RagC's GDP nucleotide through a direct hydrogen bond interaction. GTP binding to RagC triggers a small shift in the position of two of the switch I residues that "closes" the inter-space between the GTPases and prevents the Raptor claw from entering (Appendix 1) (49)

To summarize, only the RagA•GTP–RagC•GDP state is able to recruit mTORC1 because the  $\alpha$ -solenoid section of Raptor cannot interact with RagA's switch regions when GDP is bound and similarly, RagC binding to GTP prevents the Raptor claw from inserting between the Rag GTPases.

## 1.2.4 SLC38A9

The whole machinery that enables the recruitment and activation of mTORC1 at the lysosomal surface in response to intralysosomal amino acid levels, requires an amino acid sensing mechanism. This function is fulfilled by the amino acid sensor and transporter SLC38A9, located on the lysosomal membrane. It possesses 11 transmembrane domains, and an N-terminal cytosolic tail that interacts with the Rag-Ragulator complex (50).

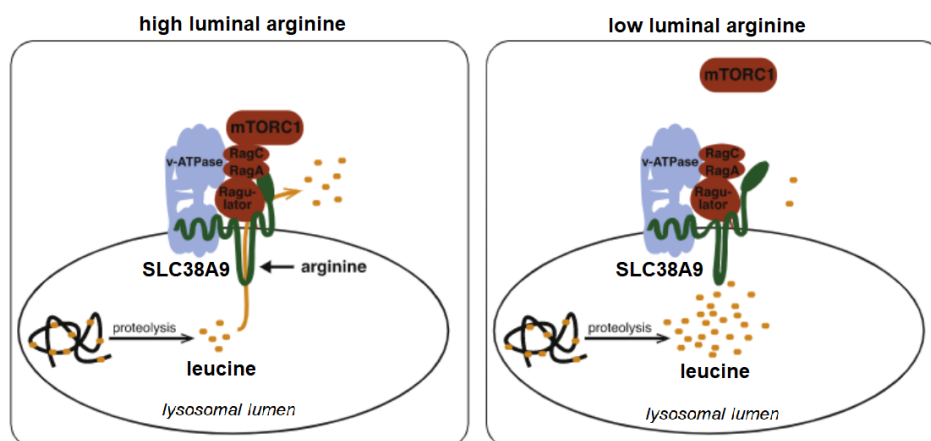


Figure 11: SLC38A9 interacts with the Rag-Ragulator complex and activates mTORC1 and transports leucine outside of the lysosome in an arginine-dependent fashion. (51)

Its arginine binding site enables it to sense intralysosomal arginine levels. Moreover, it is able when bound to arginine, to transport leucine and other essential amino acids from the lysosomal lumen into the cytosol and activate mTORC1 (Figure 11) (51,52). The cytosolic amino acids are then sensed by other proteins such as sestrins and CASTOR1, that respectively react to leucine and arginine levels in the cytosol and regulate the activity of the Rag GTPases dimer, enabling its activation (53,54) (Figure 12).

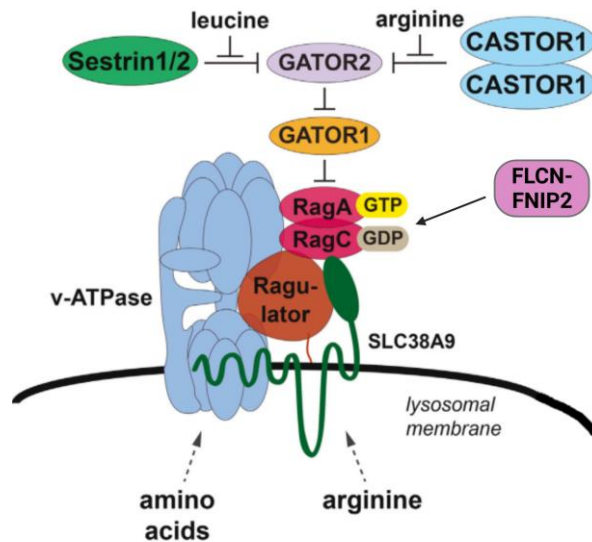


Figure 12: Summary of the key effectors of Rag GTPases activation and inhibition in response to cytosolic and intralysosomal arginine and leucine levels. (Modified from (54))

The N-terminal domain of SLC38A9 is the key of the amino-acid mediated activation of mTORC1. In amino acid starvation conditions, when no arginine is detected, this N-terminal tail was found to be inserted within the SLC38A9 transporter, in the arginine binding pocket (50). Moreover, in such conditions, FLCN-FNIP2 is bound to the Rag GTPases and unable to exhibit its GAP activity towards RagC, while GATOR2 is inhibited through the action of sestrins, enabling GATOR1 to keep the Rag GTPases inactive (Figure 12). The presence of arginine in the lysosomal lumen triggers its dissociation from the pocket, enabling it to bind the Rag-Ragulator complex. This binding disturbs the Lysosomal folliculin complex (LFC), consisting of Ragulator bound to the inactive Rags dimer, itself bound to the FLCN-FNIP2 complex (55). The disruption of the LFC triggers the GAP activity of FLCN-FNIP2 towards RagC, enabling it to shift from RagC•GTP to RagC•GDP, which as mentioned previously, will spontaneously lead to the exchange of RagA's GDP into GTP and thus result in shifting the Rag GTPases to their active state, where mTORC1 can be recruited and activated (56,57). Moreover, the transport of leucine to the cytosol enabled by SLC38A9 will inhibit the action

of the sestrins, enabling GATOR2 to inhibit GATOR1, which also results in the Rag GTPases' activation.

To summarize, the presence of arginine in the lysosomal lumen is signaled to mTORC1 through the action of SLC38A9, transporting amino acids outside lysosomes and triggering the switch of the Rag GTPases to their functionally active state, thus recruiting mTORC1 to the lysosomal surface where it is activated by Rheb to promote cell growth.

### **1.3 mTORC1 and SLC38A9 in pancreatic cancer**

Pancreatic ductal adenocarcinoma (PDAC) is one of the deadliest forms of cancer, with patients exhibiting a life expectancy of no more than 5 years for 6.7% of the cases (58). The main cause for this is the difficulty of diagnosis, due to the lack of symptoms. Thus, such cancers are usually detected at a very advanced stage, making tumor removal by surgery only possible in 15 to 20% of the cases (59). Surgery is the only efficient way to cure PDAC, that has shown to be quite unresponsive to other treatments such as chemotherapy, radiotherapy or immunotherapy, with no true improvement of the patient's life expectancy(60). Thus, more personalized therapeutic strategies are being investigated for PDAC treatment. A subpopulation of PDAC has shown to exhibit a high activation of mTOR. In such cases, its inhibition resulted in cancer cell death. The mTOR pathway could thus be an interesting therapeutic target for PDAC treatment (61,62).

The high growth rates of such pancreatic cancer cells are achieved through active scavenging of nutrients, mainly proteins, from their extracellular environment, digesting and recycling them to generate energy and produce glucose, lipids or other proteins. This results in fast tumor spreading to neighboring organs and explains the high mortality rate (63).

90% of pancreatic cancer patients exhibit oncogenic KRAS mutations, located upstream of the PI3K/Akt/mTOR pathway, thus affecting many cellular processes including cell proliferation, migration, metabolism, and autophagy (64,65).

Oncogenic Ras signaling increases nutrient uptake from the extracellular environment through macropinocytosis, a route of vital importance for KRAS-transformed cells' metabolism. It has been shown that macropinocytosis inhibition resulted in slowing the growth of such cells. (66)

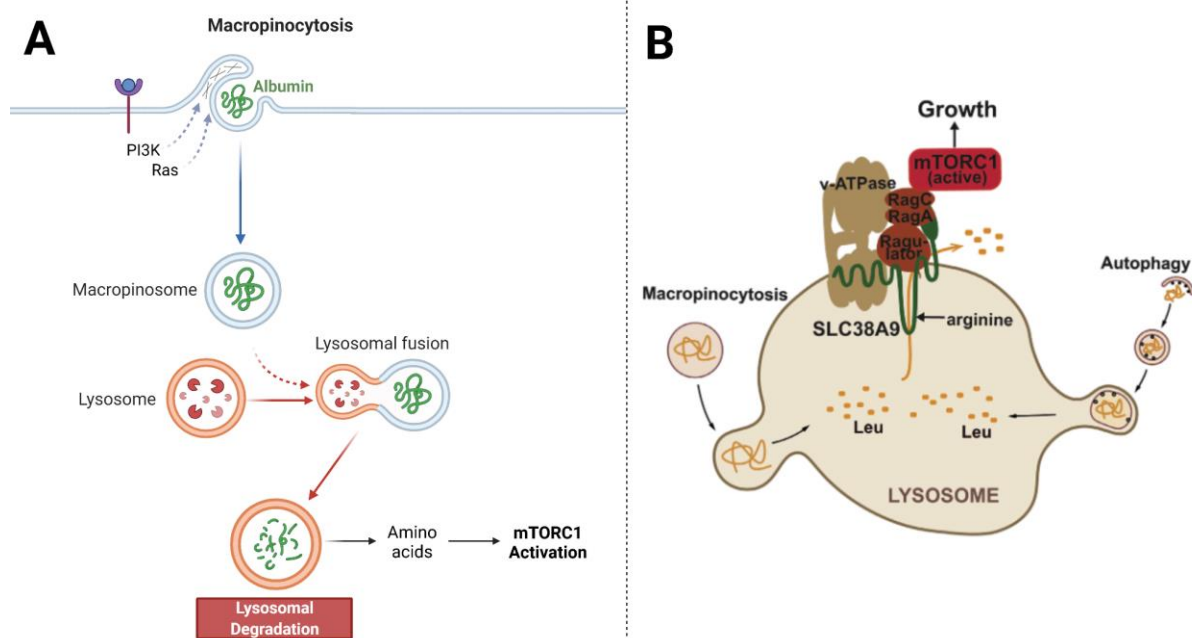


Figure 13: Macropinocytosis and lysosomal degradation of proteins, leading to mTORC1 activation. (A) Ras and PI3K induce actin-rich ruffles in the cell membrane, forming a macropinosome. The taken up albumin is digested by lysosomal enzymes after macropinosome and lysosome fusion. (B) The resulting amino acids (here leucine) are sensed and transported by SCL38A9, activating mTORC1 in an arginine-dependent fashion. (Fig. 13B from (51))

Macropinocytosis is a unique form of endocytosis that, unlike the others, is independent from both clathrin and caveolin (67,68). It instead relies on Ras and PI3K induced actin cytoskeletal rearrangement, leading to the formation of ruffles in the cell membrane (Figure 13A) (69). Albumin is here used as an example : it is taken up by the cell through macropinocytosis and later degraded by lysosomal proteases in the lysosome (Figure 13A). The amino acids resulting from this degradation are stored in lysosomes and sensed by SLC38A9, enabling the switch in the Rags nucleotide bound state and thus the translocation and activation of mTORC1.

As mentioned previously, SLC38A9 mediates the transport of amino acids, especially leucine outside of the lysosomes in an arginine-dependent fashion, making it essential for these amino acids to activate mTORC1 (Figure 13B) (70)

Thus, SLC38A9 plays an important role in fueling cancer cell growth in PDAC with oncogenic KRAS, both by using the amino acids resulting from protein scavenging to activate mTORC1 (through the Rag GTPases), but also by transporting them outside lysosomes, where they can be used as building blocks for several cell growth processes. Thus, SLC38A9 is an interesting drug target for targeted pancreatic cancer therapy.

## 2 Aim of the Study

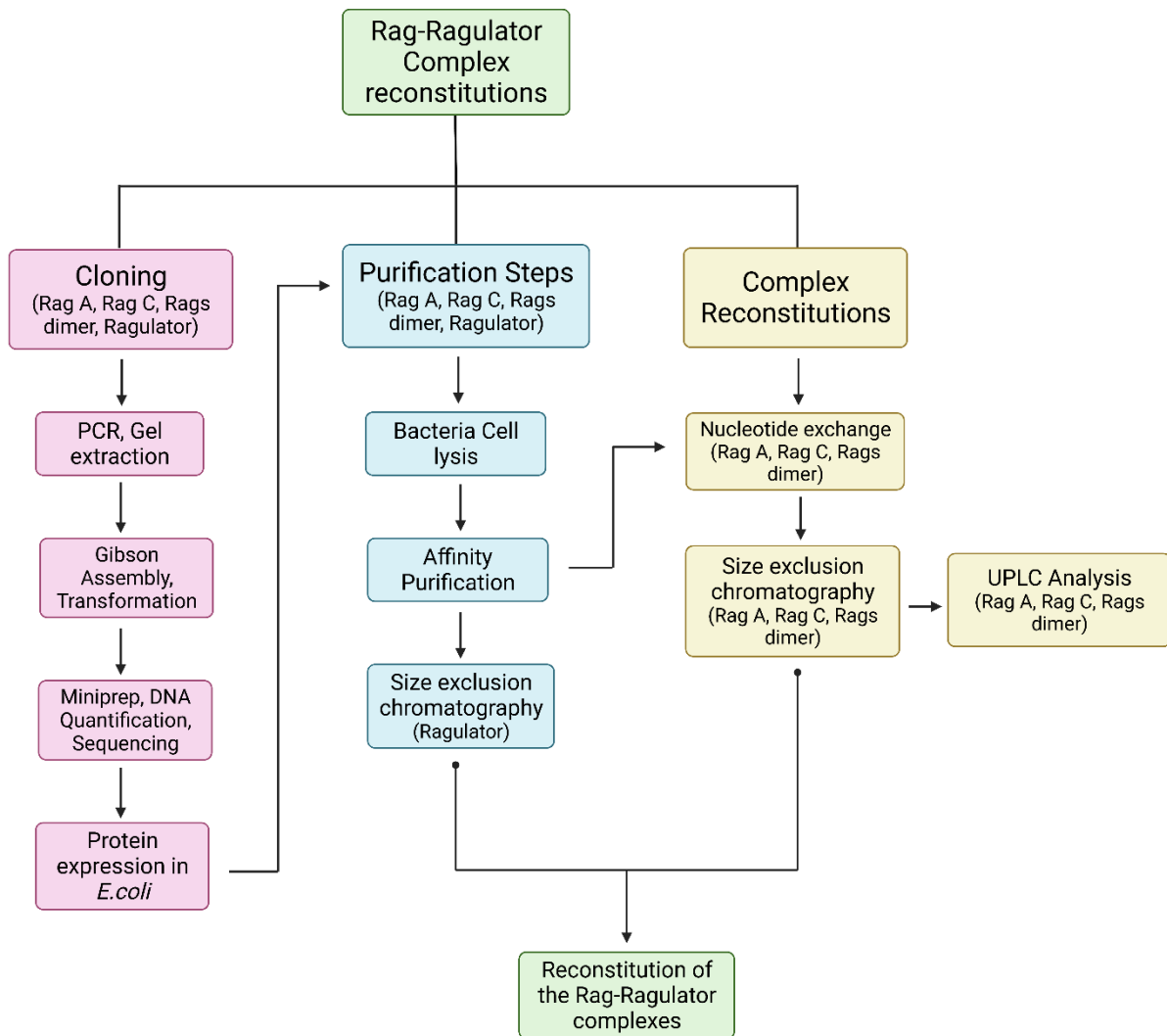
The study of the mTORC1 signaling components involved in its activation by amino acids was divided into two distinct projects.

We previously investigated the interactions that enable the Rag-Ragulator complex to recruit and activate mTORC1 at the lysosomal surface, through interaction of Raptor with the Rag GTPases heterodimer in its active RagA•GTP–RagC•GDP nucleotide-binding state. To push this study further, we want to investigate the conformational changes triggered by the change in the nucleotide-binding state of the Rag GTPases, in other words how the Rags move either towards or apart from each other depending on which nucleotides are bound to them. To do so, we aim to reconstitute the Rag-Ragulator complex in its 4 nucleotide-binding conformations : RagA•GTP–RagC•GTP ; RagA•GDP–RagC•GDP ; RagA•GDP–RagC•GTP ; RagA•GTP–RagC•GDP for their structures to be later determined using Cryo-Electron microscopy.

Interacting with the Rag-Ragulator complex, the amino-acid sensor and transporter SLC38A9 is essential to mTORC1's activation by intralysosomal amino acids. Aggressive pancreatic cancer cells, with oncogenic Kras signaling require SLC38A9 to use proteins as a food source. Taken up through macropinocytosis, they are digested in the lysosomes and the resulting amino acids are used to fuel cancer cell growth, enabling such cancers to achieve extremely high growth rates. The role of SLC38A9 in this mechanism makes it a perfect drug target for pancreatic cancer patients. The long-term aim of this project is to find a novel inhibitor to bind and inhibit SLC38A9 amino acid transport, preventing them from being released in the cytosol to be used for cancer cell growth. To do so, the first step will be to reconstitute SLC38A9 onto a membrane scaffold protein nanodisc for further structural studies.

# 3 Material and Methods

## 3.1 Reconstitution of the Rag-Ragulator Complex



*Flow chart of the Rag-Ragulator complex reconstitution project.*

## **3.1.1 Cloning of the subunits : RagA, RagC and Ragulator**

### **3.1.1.1 PCR, Agarose gel electrophoresis, Gel Extraction**

The gene inserts of RagA, RagC, the RagA–RagC dimer and Ragulator along with their respective pFloat backbones (Appendix 3), were amplified through 27 cycles of Polymerase chain reactions. A Master mix was prepared with 5X Phusion HF Buffer (Thermo fisher), dNTPs (Thermo fisher), H<sub>2</sub>O, and KAPA DNA polymerase (Roche). 0.2 μL of the corresponding DNA template, and 0.8 μL of primers were added to each reaction before putting the samples in the PCR cycler (Thermo fisher). The resulting PCR products were analyzed through Agarose gel electrophoresis, enabling the separation of the DNA fragments based on their size. The Agarose gel was prepared by dissolving 1.6 g of Agarose (Invitrogen) in 160mL 1x Tris Acetate-EDTA (TAE) buffer, supplemented with 10 μL of SYBR safe (Invitrogen). The samples were run at 140 V for 40 minutes.

After analysis, the bands corresponding to our gene inserts and vectors were excised and purified from the agarose gel using the Gel Extraction Kit and Protocol (Qiagen), to which a few adjustments were made. The agarose gel bands were dissolved in a 3x v/w of solubilization buffer at 50°C with 1000 RPM shaking. One volume of Isopropanol was added before transfer on a QIAquick spin column for centrifugation at 21 000 g for 30 minutes in a room temp benchtop centrifuge. The column was then washed with 500 μL of solubilization buffer, and 650 μL of ethanol wash buffer (PE), with 1 minute of 21 000 g centrifugation each. In order to remove any ethanol remaining from the PE buffer wash, an extra centrifugation step was performed for 1 minute at 21 000 g. The spin column was then placed into a clean 1.5mL Eppendorf tube for DNA collection, eluted with 12 μL of warm H<sub>2</sub>O. After a 5 minutes incubation the samples were spun down for 2 minutes at 11 000 g. The concentration of the obtained DNA was estimated through measurement of the sample's absorbance at 260 nm. using Nanodrop 2000 (Thermo scientific).

### 3.1.1.2 Gibson Assembly and Transformation

Gibson Assembly was used for insertion of the genes into their respective vectors. This cloning method enables to join DNA fragments with sequence similarity at the extremities without restriction enzymes, in a short, single isothermal reaction using 3 enzymatic activities: T5 Exonuclease, Phusion DNA polymerase and Taq Ligase (71).

The exonuclease, operating at 37°C recognizes the DNA sequences from 5' end to 3' end. They are then ligated by the ligase and polymerase that both operate at 50°C. The purified DNA fragments and backbones were added in equimolar concentrations to the 1.33X Gibson reaction mix (Thermo fisher), in 2 µL reactions. The reactions were then incubated for 10 minutes at 37°C, followed by 15 minutes at 50°C, after what transformation was performed (Figure 14).

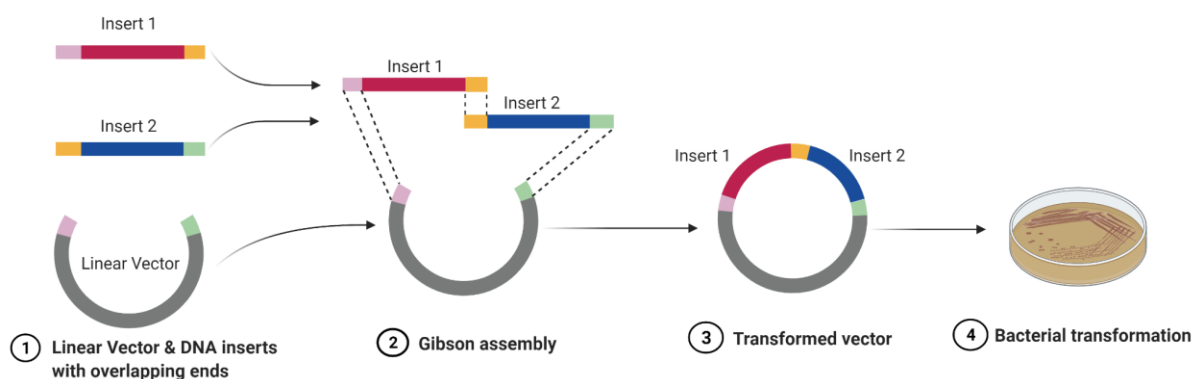


Figure 14: Gibson Assembly (adapted from Biorender)

For both RagA and RagC, the insert gene was cloned into a pFloat.cspA vector (Appendix 3) with Kanamycin resistance, conferring the protein an N-terminal Hexa-histidine Tag and a HRV-3C protease cleavage site. The insert gene of the Ragulator construct was cloned into a pFloat.assemble(AB) vector (Appendix 3) with an Hexa-histidine tag on its c7orf59 subunit and a GST-tag on the p18 subunit for affinity purification.

The recombinant ligated DNA obtained from the Gibson assembly was transformed into NEB (New England Biolabs) 10-Beta *E. coli* competent cells according to the following protocol : 0.5 µL of recombinant DNA was added to 50 µL of freshly thawed NEB 10-Beta competent cells in a 1.5 mL microtube and incubated on ice for 30 minutes. The cells were then heat shocked at 42°C for 45 seconds. 500 µL of SOC medium (Thermo fisher) were added to the

transformation reaction and cells were incubated for recovery at 37°C with shaking 200 RPM for 1 hour. The recovered cells were pelleted down by centrifugation at 3000 g and plated on an LB agar plate 50 µg/ml Ampicillin or Kanamycin (Sigma). The plates were incubated overnight at 37°C and individual colonies were picked the day after to be grown for minipreps and sequencing. The antibiotic resistance gene was placed in the insert, to avoid obtaining colonies from an empty ligated backbone. Thus, only a successfully ligated insert would result in bacterial colonies.

### 3.1.1.3 Miniprep, DNA quantification and sequencing

Individual colonies were resuspended in LB medium (Thermo fisher) and antibiotics (Ampicillin/Kanamycin) at a 1:1000 v/v dilution from a 50 µg/mL stock, i.e. 10 µL of antibiotics for 10mL of growth medium. They were grown overnight at 37°C with 200 RPM shaking in 50 mL bio-reaction tubes (Celltreat scientific). The overnights were minipreped the day after using the Qiagen miniprep kit and protocol (Appendix 4). Plasmid DNA was quantified through nanodrop measurement of Absorbance at 260 nm using Nanodrop 2000 (Thermo scientific) and sequenced by Quintarabio.

## 3.1.2 Expression and growth in LOBSTR cells

The recombinant DNA was transformed into LOBSTR (Low background strain) *E. coli* competent strain (Kerafast), with Chloramphenicol resistance, and plated on LB agar plates with 50 µg/mL Kanamycin. This strain is a good choice for expression and purification of Histidine-Tagged proteins, because of the very low production of other Histidine-rich contaminants (72) The colonies resulting from this transformation were grown as pre-cultures in Terrific Broth (TB) medium (Thermo fisher) at 37 °C for 6 hours. 10 mL of pre-culture were later added to each 2.8L growth flasks, containing 1.5 L of TB medium each in addition to 25 µg/mL of Kanamycin, 17 µg/mL Chloramphenicol and 0.025% antifoam reagent SE-15 (Sigma). The cells were grown at 37°C with 200 RPM shaking.

The gene expression of the Rag GTPases was controlled by a Cold shock protein A (*cspA*) promoter, a small bacterial protein whose expression is stimulated by cold shock (73,74).

Once the cells OD<sub>600</sub> exceeded 2.0, they were cold shocked through incubation on iced water for 30 minutes prior to induction of protein expression with 0.5 mM isopropyl β-D-1-thiogalactopyranoside (IPTG). Cells were then grown at 15°C and harvested 48h later in 1L bottles by centrifugation at 6000 g for 8 minutes in a JLA-8.1000 rotor (Beckman Coulter). The cell pellets were frozen in Liquid Nitrogen (LN<sub>2</sub>), weighed, and stored at -20°C.

The Ragulator construct's expression is controlled by a bacteriophage T7 RNA polymerase. Its transcription is controlled by a lac promoter, on which a lac repressor is bound, inhibiting the translation of the T7 RNA polymerase. The induction of protein expression through the addition of IPTG inhibits the lac repressor, thus triggering the polymerase's translation and simultaneously translating of our protein of interest (75). After their OD<sub>600</sub> exceeded 2.0, cells were incubated at 4°C for 45 minutes and protein expression was later induced with 0.5mM IPTG. Cells were then grown at 18°C and harvested 24 hours later in 1L bottles, also by 8 minutes centrifugation at 6000 g, in a JLA-8.1000 rotor . The pelleted cells were frozen in LN<sub>2</sub>, weighed and stored at -20°C.

### **3.1.3 Purification of the Rag GTPases and Ragulator constructs**

The entire protein preparation and purification processes were performed at 4°C to avoid any protein degradation. Samples were taken at each step, from cell lysis to gel filtration and supplemented with 5x SDS-loading dye for SDS-PAGE analysis.

#### **3.1.3.1 Bacteria cell lysis**

Lysis buffer A and B (Appendix 5) were added to the frozen cell pellets of the Rag GTPases and Ragulator respectively, at a 1:3 w/v ratio. The cells were supplemented with lysozyme and stirred at 4°C for 1 hour for initial lysis. In the case of the Rag GTPases constructs, the pellets in lysis were supplemented with high quality GTP nucleotides and MgCl<sub>2</sub> (Appendix 5, Lysis Buffer A), to improve the stability of the constructs during the cell lysis and avoid protein degradation. In order to ensure the breakage of bacterial cell walls, the pre-lysates

were then transferred to a microfluidizer reservoir operating at 4°C, pre-equilibrated with cold Phosphate-buffered saline (PBS) (Thermo fisher). Cells were lysed by 3 passages under 15 000 PSI air pressure, and the final PBS wash was added to the total lysate.

The proteins to be purified are soluble, the debris from cell lysis were thus pelleted through 1 hour centrifugation of the lysate at 30 000 g in a JLA-16.250 rotor (Beckman Coulter) at 4°C. The supernatant was then passed through a 0.45 µm bottle-top-filter (Corning) to remove any remaining debris before binding to affinity resin.

### 3.1.3.2 Affinity Chromatography of the Rag GTPases

For the RagA, RagC, and Rags dimer constructs, the spun-filtered lysate was supplemented with 20 mM imidazole and 2 mL bed volume of Nickel (Ni-NTA) agarose resin (Qiagen) previously equilibrated with 3 x 10 mL of binding/wash buffer A (50mM HEPES pH 7.0, 100 mM NaCl, 20 mM imidazole, 0.5 mM TCEP, 0.5 mM PMSF, 2 mM MgCl<sub>2</sub>, 0.1% Tween20) and incubated for binding at 4°C for an hour on a roller mixer.

The resin-lysate mix was then passed through a 50 mL affinity chromatography column (CrystalCruz) to capture the protein-bound Ni-NTA resin. The flowthrough was discarded, and the resin was washed in the following order with 150 mL of wash buffer A, 200 mL of ATP/High salt buffer A (50mM HEPES pH 7.0, 300 mM NaCl, 5mM ATP, 20 mM imidazole, 0.5 mM TCEP, 0.5 mM PMSF, 20 mM MgCl<sub>2</sub>, 0.1% Tween20) and at last 50 mL of wash buffer A. The ATP/High salt wash is used to remove contaminants that cannot be removed with regular buffer wash, such as Chaperone proteins, that bind polypeptide chains and stabilize them, often acting as a folding helper (76). As our proteins are being purified for structural studies, it is important to have a final protein sample as pure as possible. In a 25 mL volume of wash buffer A, the resin-bound protein was supplemented with 0.18 µM of GST-HRV3C protease and incubated overnight in the column at 4°C on a roller-mixer for cleavage of the His-Tag. The cleavage flowthrough was collected in a 50 mL falcon tube, and the resin was washed 3 times with 5 mL of wash buffer A. Samples were taken at each step : 40 µL in ½ Column volume (CV) of wash buffer A + 10 µL of 5x SDS-loading dye (the resin samples were taken from stirred resin with a cut pipet-tip). An SDS-PAGE analysis was run to verify protein expression, purification and release from the resin. The wash and flowthrough fractions of the Rag GTPases constructs were concentrated before nucleotide exchange, on Amicon Ultra 15 mL (Millipore) regenerated cellulose membrane, with a 10K

molecular weight cut-off (MWCO) for RagA and RagC, and 30K for the Rags dimer. The concentration was estimated given the protein's absorbance at 280 nm its molar extinction coefficient (calculated using the ProtParam tool in ExPASy) and molecular weight : respectively 29910 and 37015.21 Da for RagA ; 37105 and 44770.16 Da for RagC ; 59250 and 80795.09 Da for the Rags dimer.

### 3.1.3.3 Affinity Chromatography of Ragulator

The spun-clarified lysate containing the Ragulator construct was at first incubated for 2 hours on a roller mixer at 4°C, with 10 mL bed volume of GSH resin pre-equilibrated with wash buffer B (50mM HEPES pH 7.5, 100 mM NaCl, 0.5 mM TCEP, 0.5 mM PMSF, 0.1% Tween20). The resin-bound protein was then passed through a 50 mL affinity chromatography column and washed with 200 mL of wash buffer B , 250 mL of ATP/High salt buffer B (50mM HEPES pH 7.5, 300 mM NaCl, 5mM ATP, 0.5 mM TCEP, 0.5 mM PMSF, 0.1% Tween20), and finally 50 mL of wash buffer B. In a 30 mL volume, the resin-bound protein was supplemented with 2.69 µM of His6-3C protease and 0.45 µM of His7-TEV protease and incubated overnight at 4°C on a roller-mixer for cleavage of p18's GST-tag and c7orf59's hexa-histidine tag. Similarly as for the Rag GTPases, the cleavage flowthrough was collected in a 50 mL falcon tube, and the resin was washed 3 times with 5 mL of wash buffer B, collected in a separate falcon tube. Samples were taken at each step : 40 µL in ½ CV of wash buffer B + 10 µL 5x SDS-loading dye (the resin samples were taken from stirred resin with a cut pipet-tip) and ran on SDS-PAGE analysis.

In order to remove the His-Tagged proteases, the cleavage flowthrough and wash fractions were pulled together and incubated with 2.5 mL bed volume of Ni-NTA resin, for 1 hour at 4°C on a roller mixer. The protein-bound resin was then again passed through a 50 mL filter column and the flowthrough, containing our Ragulator complex free of proteases contamination was collected, along with the 3 buffer washes of 5 mL each. The flowthrough and washes were pulled together and concentrated down to 1 mL on an Amicon Ultra 15 mL, 30K MWCO (Millipore), regenerated cellulose membrane for size exclusion purification. The protein concentration was then estimated through absorbance measurement at 280 nm using Nanodrop given Ragulator's molar extinction coefficient 34840 (calculated using the ProtParam tool in ExPASy) and molecular weight 65107.01 Da.

### 3.1.3.4 SDS-PAGE Analysis

All protein samples from the affinity purifications (and later size exclusion chromatography purifications) were supplemented with 5x SDS denaturing loading dye and incubated at 95°C for 3 min, before 8 µL of each sample was applied per well to Bis-Tris 4-12% gels (Invitrogen), next to 4 µL of color-prestained 10-250 kDa protein standard (NEB), in 1x MES buffer (50/50 of fresh and used) (Thermo fisher), supplemented with 5 mM of Sodium bisulfate (Spectrum Chemical). The gels were run at 160V for 60 minutes. In the case of SLC38A9, whose purification will be detailed later, the samples were run in 1x MOPS buffer (Thermo fisher) at 180V for 60 minutes. The gel was then rinsed with distilled water and boiled before staining with InstantBlue® Coomassie Protein Stain (Abcam).

### 3.1.3.5 Size exclusion purification

As previously mentioned, the protein samples of Ragulator and the post-nucleotide exchanged Rags were concentrated down to a 1 mL on regenerated cellulose membranes with a molecular weight cut-off no larger than half the molecular weight of the purified proteins. The samples were then centrifuged at 21 000 g for 10 min in 1.5 mL tubes, to pellet any debris. The resulting supernatants were manually loaded with a syringe onto an Äkta purification system (Figure 15) via a 2.0 mL loop and injected at a 0.5 mL/min rate on a Superdex 200 16/600 column (Sigma), pre-equilibrated with 1.1 CV of SEC running buffer (Appendix 5). Proteins were eluted at a 1 mL/min rate, in 96-deep well blocks with a fixed fractionation of 1mL, starting at 0.27 CV.

## Fast Protein Liquid Chromatography

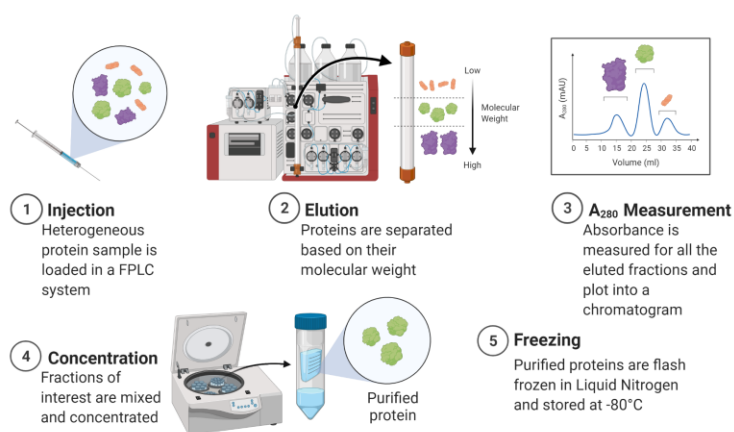


Figure 15: Steps of Fast protein liquid chromatography on an AKTA system. (Adapted from Biorender)

Size exclusion chromatography (SEC), also called gel filtration separates proteins based on their molecular weight (size). The columns contain small pores, in which smaller proteins will be trapped while larger proteins will flow faster. The low molecular weight proteins will thus be eluted later than the larger molecular weight proteins. It also enables to evaluate the stability and folding of the purified proteins based on their size exclusion profile (peak) (77). The fractions corresponding to the different protein peaks were run on SDS-PAGE analysis and those containing our purified constructs were pulled and again concentrated on regenerated cellulose membranes with the corresponding MWCO : 30 kDa for Ragulator and the RagA–RagC dimer and 10 kDa for the single Rag GTPases constructs. The protein concentration was estimated through absorbance at 280 nm using Nanodrop, based on the given molecular weight and molar extinction coefficient calculated using the ProtParam tool in ExPASy. An average was made with 4 measurements of diluted sample after blanking the machine with SEC buffer (Appendix 5). The concentrated protein samples were then supplemented with 10% glycerol and flash frozen in LN<sub>2</sub> in 50 µL aliquots and stored at -80°C for later use.

### 3.1.4 Rag-Ragulator complex reconstitutions

The Rag-Ragulator complex is aimed to be reconstituted in its 4 different nucleotide-binding states : RagA•GTP–RagC•GTP ; RagA•GDP–RagC•GDP ; RagA•GDP–RagC•GTP and RagA•GTP–RagC•GDP. The purified Rag GTPases are heterogeneously bound to GTP and

GDP nucleotides, as it is in nature. Thus, the best way to ensure them to be bound to specific nucleotides is to “manually” exchange them, with GDP and GppNHp nucleotides. GppNHp being a non-hydrolysable GTP analog (Figure 16), this will enable to lock the Rag GTPases in their GTP bound conformation. Nucleotide exchange reactions were then performed on RagA and RagC after affinity purification before size exclusion chromatography.

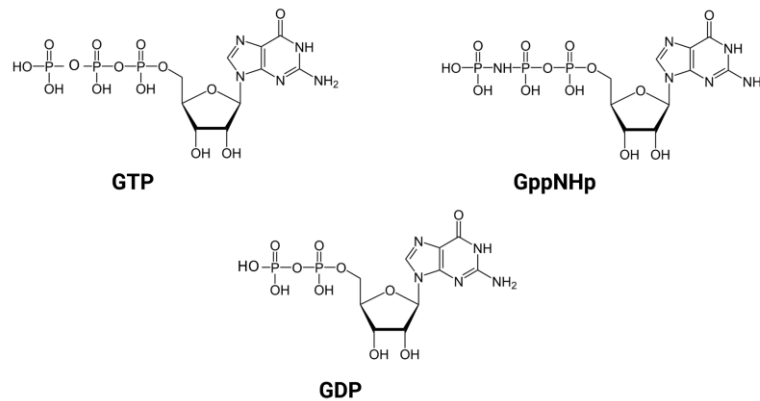


Figure 16: Molecular structures of GTP, GDP and GppNHp nucleotides.

### 3.1.4.1 Nucleotide exchange on RagA

The concentrated sample of wild type RagA, obtained after the His-affinity purification, was exchanged with both GDP and GppNHp separately in two distinct reactions, enabling to obtain two different nucleotide-bound RagA constructs : RagA•GppNHp and RagA•GDP. The exchange was made in a 1:5 MgCl<sub>2</sub>/EDTA molar ratio. Mg<sup>2+</sup> ions play a key role in the binding of nucleotides to the binding pocket of the Rag GTPases. EDTA removes MgCl<sub>2</sub> which disturbs the nucleotides binding interactions, removing it from the pocket. Thus, EDTA will enable to remove the previously bound nucleotides while the presence of Mg<sup>2+</sup> will enable the rebinding of the added GDP and GppNHp nucleotides.

The total 1 mL reaction consisted of 200 nmol of the purified RagA, incubated with 20 fold - 4000 nmol of high quality GppNHp and GDP nucleotides, 4 mM MgCl<sub>2</sub> and 20 mM EDTA, supplemented with 50 mM GluArg. The Rag GTPases were purified in the presence of MgCl<sub>2</sub>, so a bit extra was added to reach the 4 mM concentration and the reaction was topped up with H<sub>2</sub>O. The exchange reactions were incubated overnight at 4°C, and ran on gel filtration the next day.

### 3.1.4.2 Nucleotide exchange on RagC

In the case of RagC, the nucleotide exchanges were also performed on the concentrated sample resulting from His-affinity purification. The exchange with GDP was performed following the exact same protocol as for RagA, using MgCl<sub>2</sub> and EDTA. Nevertheless, in the case of exchanging RagC with GppNHp, a less nucleotide-consuming protocol was favored, using Calf Intestinal alkaline Phosphatase (QuickCIP) (NEB). This enzyme specifically degrades the GTP and GDP nucleotides present in the binding pocket of RagC, leaving it free for GppNHp to bind. As the reaction was this time catalyzed by an enzyme, a 10-fold excess of GppNHp was sufficient for a complete exchange. 200 nmol of wild-type RagC were added to 2000 nmol of GppNHp high quality nucleotides (Jena Bioscience), in exchange buffer : 10 mM HEPES pH 7.5, 50 mM NaCl, 150 mM (NH<sub>4</sub>)<sub>2</sub>SO<sub>4</sub>, 0.05 mM ZnCl<sub>2</sub>, 5 mM DTT. The Quick CIP enzyme was added - (NEB), at a dose of 0.1 U per nmol from a 5 U/μL stock. The reaction was topped up with H<sub>2</sub>O up to a volume of 1 mL, incubated overnight at 4°C and ran on gel filtration the next day.

### 3.1.4.3 Nucleotide exchange on the Rags dimer

Similarly as for RagA, 200 nmol of the GTPases dimer RagA – RagC was exchanged with high quality GDP nucleotides, added in a 20 fold molar excess, in a 1:5 molar ratio of MgCl<sub>2</sub> and EDTA, supplemented with 50mM GluArg in a 1 mL reaction volume. The reaction was again run on gel filtration after an overnight incubation at 4°C.

### 3.1.4.4 Ultra Performance Liquid Chromatography

After each nucleotide exchange, the Rags were purified through size exclusion chromatography and concentrated to be used in complex reconstitutions. In order to check the successful exchange with the chosen nucleotides, the latters were extracted from the purified exchanged Rags to be run on Ultra Performance Liquid Chromatography (UPLC). 3 nmol of the exchanged Rag GTPases were taken into a 200 μL PCR tube, and the volume was topped up to 44 μL by SEC buffer addition (Appendix 5). 2.5 μL of 10% HClO<sub>4</sub> was then added to a

spin-column filtrate to precipitate the protein, followed by 3.5  $\mu\text{L}$  of 2 M  $\text{CH}_3\text{COONa}$  pH 4.0 to raise the pH. The precipitated protein was pelleted through centrifugation at 21 000 g for 5 minutes. The supernatant containing the 50  $\mu\text{L}$  nucleotide solution was transferred to an insert and placed in a UPLC vial (Waters). 5  $\mu\text{L}$  of each nucleotide sample was then injected and run on a 0.2 mL C18 UPLC column (Thermo fisher), monitoring the nucleotide absorbance at 254 nm (nucleotides absorb light at 254 nm), using the following standards :

- 500  $\mu\text{M}$  GTP - Guanosine 5'-triphosphate sodium salt hydrate  $\geq 95\%$  (HPLC) (Sigma)
- 500  $\mu\text{M}$  GDP - Guanosine 5'-diphosphate sodium salt Type I,  $\geq 96\%$  (HPLC) (Sigma)
- 500  $\mu\text{M}$  Gpp(NH)p,  $\geq 95\%$  (HPLC) (Jena Bioscience)

#### 3.1.4.5 Reconstitution and purification of the Rags-Ragulator complexes

To allow spontaneous reconstitution of the Rags-Ragulator complex, the Rag GTPases were incubated overnight at 4°C with the Ragulator complex at a 1:1:3 ratio, 15 nmol of RagA, 15 nmol of RagC and 45 nmol of Ragulator. Because of its tail-like structure, the p18 subunit of Ragulator can easily be degraded by proteases which is why this ratio was favored to a 1:1:1 ratio increasing the chances of getting a fully assembled complex. The total reaction volume was 250  $\mu\text{L}$ , to enable the reconstituted complex to be loaded directly, without any further concentration needed via a 250  $\mu\text{L}$  syringe on a Superdex200 10/300 column (Sigma) pre-equilibrated with 1.1 CV of SEC buffer (Appendix 5). The sample was directly injected through a 500  $\mu\text{L}$  injection loop emptied with 1 mL was injected at a 0.25 mL/min rate, and eluted at a 0.5 mL/min rate with a fixed fractionation of 0.3 mL into 96-deep well blocks, starting at 0.28 CV. The reconstituted complex containing fractions were then pulled and concentrated on a 30K MWCO regenerated cellulose membrane, and the concentration was estimated through nanodrop measurements given the complex's molar extinction coefficient 109620 calculated using ProtParam tool in ExPASy, and molecular weights given for the 4 nucleotide-binding states : 146930.45 Da for RagA•GppNHp – RagC•GppNHp, 146850,50 Da for both RagA•GDP – RagC•GppNHp and RagA•GppNHp – RagC•GDP, and finally 146770.49 Da for RagA•GDP – RagC•GDP.

## **3.2 Reconstitution of SLC38A9 into a membrane scaffold protein nanodisc**

Membrane proteins tend to be extremely unstable when outside of their natural lipid bilayer environment. This is a challenge for structural studies, as protein imaging requires the protein to be as stable and nicely folded as possible (78). Therefore, membrane protein SLC38A9 is to be reconstituted in a membrane scaffold protein (MSP) nanodisc using NW11 as an MSP, giving a nanodisc of an 11 nm diameter, reconstituting the natural environment of the protein to facilitate later structural studies (78)

### **3.2.1 Expression and purification of the membrane scaffold protein NW11**

#### **3.2.1.1 Expression of NW11**

The NW11 construct was designed as follows: NW11-Cys-Avi-3C-His10 with a deca-histidine-tag for his affinity purification, an HRV3C protease cleavage site to facilitate it's release from Ni-NTA resin, an Avi-Tag to enable future protein biotinylation and a Cysteine-Tag to be targeted in drug screening experiments (79). The construct was amplified through PCR, purified from Agarose gel and cloned into a pFloat.T7 vector (Appendix 3) through Gibson assembly. The resulting DNA was cloned into NEB10 beta competent cells using the previously described transformation protocol. The DNA from the resulting colonies was isolated through miniprep and sequenced to ensure the rightful plasmid assembly.

The assembled final plasmid was then transformed into LOBSTR (Low background strain) *E. coli* competent strain with Chloramphenicol resistance, on LB agar plates with 50 µg/ml Kanamycin. The colonies resulting from this transformation were grown in TB medium as 10 mL pre-cultures at 37 °C for 6 hours. The pre-cultures were later added to six 2.8L growth flasks, each containing 1.5L of TB medium in the presence of Kanamycin 25 µg/mL, Chloramphenicol 17 µg/mL and 0.025% antifoam reagent SE-15. The cells were grown at 37°C with 200 RPM shaking for 17 hours. The protein was expressed with the T7 RNA polymerase system. After their OD<sub>600</sub> exceeded 2.0, cells were incubated at 4°C for 45 minutes and protein expression was induced with 0.5mM IPTG. Cells were then grown at

18°C and harvested after 24 hours in 1L bottles by centrifugation for 8 minutes at 6000 g, in a JLA-8.1000 rotor. The pelleted cells were frozen in LN<sub>2</sub> in a 500 mL square bottle, weighed and stored at -20°C.

### 3.2.1.2 Purification of NW11

The cells were thawed and stirred in 1:3 w/v ratio of lysis buffer C (Appendix 5) supplemented with lysozyme, at 4°C for 1 hour for initial lysis. The pre-lysate was then transferred to a microfluidizer reservoir operating at 4°C, pre-equilibrated with cold PBS and passed 3 times under 15 000 PSI air pressure, to break the bacterial cell walls. The final PBS wash was added to the total lysate. The cell lysate was then spun down at 30 000 g for 1 hour at 4°C in a JLA-16.250 rotor. The supernatant containing the membrane scaffold protein NW11 was passed through a 0.45 µm bottletop-filter to remove any remaining debris, and the spun-clarified lysate was supplemented with 20mM imidazole and incubated with 1.5 mL bed volume of Nickel-NTA agarose resin pre-equilibrated with 3 x 10 mL of wash buffer C (50 mM HEPES pH 7.0, 100 mM NaCl, 0.5 mM TCEP, 0.5 mM PMSF, 20mM imidazole, 0.1% Tween) for 1 hour at 4°C on a roller mixer. The protein-bound resin was then passed through a 50 mL affinity chromatography column, and washed with 150 mL of wash buffer C, 200 mL of ATP/High salt buffer C (50 mM HEPES pH 7.0, 500 mM NaCl, 0.5 mM TCEP, 0.5 mM PMSF, 20mM imidazole, 5mM ATP, 0.1% Tween) and finally 50 mL of wash buffer C. In a 25 mL volume (of wash buffer C), the resin-bound protein was supplemented with 1.2 µM of GST-HRV3C protease and incubated overnight in the column placed at 4°C on a roller-mixer for cleavage of its deca-histidine tag. The cleavage flowthrough was collected in a 50 mL falcon tube, and the resin was washed with 20 mL of wash buffer C, separately collected. Samples were taken at each step and ran on SDS-PAGE at 160 V for 60 minutes to verify protein expression, purification, and release from the resin. The cleavage flowthrough and wash were then pulled together and concentrated on Amicon Ultra 15 mL, 10K MWCO, regenerated cellulose membrane (Millipore). The final concentration was estimated through absorbance measurement at 280 nm using Nanodrop 2000 (Thermo Scientific), based on the given molecular weight 24146.3 Da and molar extinction coefficient 23950 calculated using the ProtParam tool in ExPASy. The protein was supplemented with 10% glycerol and flash frozen in LN<sub>2</sub> and stored at -80°C for later use.

## 3.2.2 Expression, Isolation and Purification of SLC38A9

### 3.2.2.1 Expression of SLC38A9

SLC38A9 was expressed in mammalian cells with a single Flag-tag. The stable cell line for expression was generated through lentiviral transduction of SLC38A9's gene in Expi293 cells adapted to Freestyle 293 medium with 1% serum and 1% PenStrep. Similarly as other lysosomal proteins, SLC38A9 possesses glycans on its intralysosomal side to protect it from degradation by lysosomal proteases (80,81).

In order to shorten the glycans and facilitate later drug screening experiments, the cells were treated with 1  $\mu$ g/mL Kifunensine during culture and expansion. Kifunensine is a drug that inhibits  $\alpha$ -mannosidase, an enzyme with a crucial role in N-glycans processing and polymerization (82). Cells were grown in large volumes of 8 to 12 Liters at 37°C, with 80% humidity and 8% CO<sub>2</sub> and shaking at 125 rpm. Cells were supplemented with 4 mM VPA 24 hours after reaching a 2 millions/mL confluency, and harvested 48 hours later in 1L bottles at 4000 g in a JLA-8.1000 rotor. The cells pellets were weighed and frozen in LN<sub>2</sub> and stored at -20°C.

### 3.2.2.2 Cell lysis and membrane isolation

Cells were later thawed in a 1:4 w/v ratio of lysis buffer D (Appendix 5), stirring for 1 hour at 4°C for initial lysis. In order to complete cell lysis and disruption, the pre-lysate was then transferred to a microfluidizer reservoir operating at 4 °C, and passed 3 times under 15 000 PSI air pressure. Cold PBS was used for initial buffer equilibration and final wash. The resulting lysate was spun down at 30 000 g in a JLA-16.250 rotor for 45 min at 4°C, to pellet as many debris as possible before membranes isolation. The supernatant was then transferred to new ultracentrifuge tubes pre-chilled on ice and centrifuged at 165 000 g for 1 h 30 at 4°C in a Ti45 rotor (Beckman), to pellet the cell membranes. The supernatant was discarded and the pelleted membranes were resuspended in membrane resuspension buffer, added at a 1:5 w/v ratio, containing 50 mM HEPES pH 8.0, 500 mM NaCl, 20% glycerol, 1 mM TCEP, 1 mM PMSF, ~1 % DDMw/v and 1 tablet of half dose EDTA-free protease inhibitors (Roche Ultra) per 50 mL of buffer. The membranes were left stirring in the buffer at 4°C for 16 hours

until complete homogenization. The solubilization mixture was then transferred to clean ultracentrifuge tubes and spun down at 165 000 g for 30 minutes at 4°C in a Ti-45 rotor for final debris removal. The resulting supernatant was used for binding to 1.5 mL of bed volume of Anti-FLAG M2 Affinity Gel (Sigma), pre-equilibrated with wash buffer D and incubated for 2 hours at 4°C on a roller mixer.

### 3.2.2.3 SLC38A9 Purification

The resin-bound protein was then captured on a filter column and washed with 30 mL and later 70 mL of binding wash buffer D (50 mM HEPES pH 8.0, 150 mM NaCl, 10% glycerol, 0.5 mM TCEP, 1 mM PMSF, 0.5mM DDM), and finally 75 mL of ATP/High salt Buffer D (50 mM HEPES pH 8.0, 500 mM NaCl, 10% glycerol, 0.5 mM TCEP, 1 mM PMSF, 0.5 mM DDM, 5mM ATP), followed with 20 mL of wash buffer D. The Flag-SLC38A9 was then eluted from the resin with 5 rounds of 10 minutes incubations with 4 mL of Elution buffer (50 mM HEPES pH 8.0, 150 mM NaCl, 10% glycerol, 0.5 mM TCEP, 1 mM PMSF, 0.5mM DDM, 175 µM of 3xFLAG peptide). Similarly as for previous purifications, samples were taken at each step, and ran on SDS-PAGE in 1x MOPS buffer (Thermo fisher) at 180V for 60 minutes to verify protein expression, purification and release from the resin. The elution fractions were then supplemented with 50mM GluArg and concentrated on Amicon Ultra 15 mL, 30K MWCO, regenerated cellulose membrane (Millipore), down to 0.5 mL to be run on size exclusion chromatography. Glycans being known to have an important role in protein stability (83), this will also enable to assess the overall stability and folding of the protein after its glycans have been shortened through Kifunensine treatment.

After a spin at 21 000 g to remove any debris or precipitated protein, the concentrated protein sample of SLC38A9 was injected onto a Superdex 200 10/300 column (Sigma) through a 1 mL injection loop into an Äkta purification system and eluted at a 0.5 mL/min rate with Size exclusion buffer (25 mM HEPES pH 8.0, 150 mM NaCl, 0.5 mM TCEP, 0.04% DDM). After the size exclusion run, the fractions were analyzed through SDS-PAGE electrophoresis. Those corresponding to the SLC38A9 protein peak were pulled and concentrated on 30K MWCO Amicon regenerated cellulose membranes. The protein concentration was estimated through absorbance at A280 using Nanodrop, based on the given molecular weight 64793.61 Da and molar extinction coefficient 88240 calculated using the ProtParam tool in ExPASy.

The protein was supplemented with 10% glycerol and flash frozen in LN<sub>2</sub> and stored at -80°C for later use.

### **3.2.3 Reconstitution of SLC38A9 into the NW11 nanodisc**

#### **3.2.3.1 Determining the ideal lipid composition**

Human membranes contain a variety of lipids. In order for the reconstituted nanodisc to be as representative as possible, the lipid composition must be as close to the one of human lysosomes as possible. Endosomal membranes appear to contain 30% of Phosphatidylcholine (PC), 30% of Cholesterol (CHS), 15% of Sphingomyelin (SM), 11% of Phosphatidylethanolamine (PE), 7% of Phosphatidylinositol (PI) and 7% of bis(monoacyl-glycero) phosphate (BMP) (84). Though, in the case of lysosomes, BMP doesn't seem to be a part of the outer lysosomal membrane composition and is thought to be sitting on the intralysosomal part of the membrane (85).

The following lipid composition was tried for nanodisc assembly, based on the composition of endosomal membranes and the available lipids:

- 42% (21µmol) of zwitterionic phosphatidylcholine (POPC) (Avanti),
- 16% (8µmol) of Positively charged phosphatidylethanolamine (POPE) (Avanti),
- 42% (21µmol) of Cholesterol (CHS)

at different NW11:Lipids ratios (1:25, 1:50, 1:75, 1:100, 1:150 and 1:200) to determine which one would give the best nanodisc assembly and the cleanest separation on gel filtration. Lipids were dissolved in 25 mM HEPES pH 7.5 and 300 mM sodium cholate to a 100 mM stock solution (3 x excess of detergent), and sonicated to get rid of micelles. These stock solutions were then used in nanodisc reconstitution trials with NW11.

30 µM of NW11 was added to lipids in buffer (25 mM Hepes pH 8.0, 150 mM NaCl) with a final sodium cholate concentration of 30mM, and incubated at room temperature for 30 minutes. 70 mg of biobeads, previously washed with methanol, water and SEC buffer (Appendix 5) were added to the reaction and incubated overnight at 4°C for detergent removal and nanodisc assembly. The reconstitution sample of a 100 µL total volume, was then spun down on a 2.2 µm spin filter at 21 000 g to remove biobeads and any “solid debris”

before injection of the size exclusion column. The resulting eluate was then again spun down for 10 min at 21 000 g before injecting 25  $\mu$ L on a 3.2/300 superose6 column (Sigma) for size exclusion chromatography, eluting with the nanodisc reconstitution SEC buffer (Appendix 5).

The same protocol was then tried with SLC38A9, this time with two different lipids compositions:

- 42% of POPC (21 $\mu$ mol), 16% of POPE (8 $\mu$ mol), 42% of CHS (21 $\mu$ mol)
- 35% of POPC (17.5 $\mu$ mol), 13% of POPE (6.5 $\mu$ mol), 35% of CHS (17.5 $\mu$ mol), and 17% of SM (8.5 $\mu$ mol)

And 3 molar ratios of SLC38A9:NW11:Lipids

- 1:10:250
- 1:10:500
- 1:10:750

The resulting samples were also run on gel filtration on a 3.2/300 superose6 column, eluted with the same buffer SEC buffer (Appendix 5)

### 3.2.3.2 Nanodisc reconstitution

These trials enabled to optimize of the reconstitution protocol. The 1:10:750 ratio was favored and used for the final reconstitution of SLC38A9 into the NW11 nanodisc. The aim is for each molecule of NW11 to be loaded with one SLC38A9 molecule. The separate components were added in the following order in a 250  $\mu$ L reaction.

- 1) 7.5 mM POPC:POPE:CHS
- 2) Size Exclusion buffer (25 mM Hepes pH 8.0, 150 mM NaCl, 0.5 mM TCEP)
- 3) Cholate buffer (25 mM Hepes pH 8.0, 150 mM NaCl, 0.5 mM TCEP, 200 mM sodium cholate)
- 4) 9  $\mu$ M SLC38A9
- 5) 90  $\mu$ M NW11

The mixture was incubated on ice for 1 hour, before addition of 175 mg of Biobeads previously washed in 1 mL rounds, 4 times with methanol, 3 times with H<sub>2</sub>O, and 2 times with size exclusion buffer. After 30 minutes incubation on ice, the tube containing the reconstitution mixture and the biobeads was incubated for 3 hours on a roller-mixer at 4°C

(86). It was observed in the reconstitution trials that biobeads tend to add an extra volume ~25  $\mu\text{L}$ , which was taken into account in the total reaction volume. The reconstituted nanodiscs mixture was then transferred to a 1.5 mL tube containing a 0.45  $\mu\text{m}$  spin-filter and spun down at 21,000 g for 2 min to remove all biobeads. The filtered nanodiscs were again centrifuged at the same speed for 10 min to pellet any precipitated protein before loading onto a Superdex200 10/300 column for size exclusion chromatography. The peaks resulting from this purification were analyzed through SDS-PAGE. Those containing the reconstituted SLC38A9 loaded nanodisc were pulled and concentrated on 30K MWCO Amicon regenerated cellulose membrane. The protein concentration was estimated through absorbance at 280 nm using Nanodrop, based on the given molecular weight 113050.18 Da. and molar extinction coefficient 136140 calculated using the ProtParam tool in ExPASy. The concentrated protein was then flash frozen in  $\text{LN}_2$  and stored at  $-80^\circ\text{C}$  for structural studies.

## 4 Results and Discussion

### 4.1 Rag-Ragulator Complex reconstitution

#### 4.1.1 Cloning, transformation and sequencing

The genes for RagA, RagC and Ragulator were successfully amplified through PCR, inserted and ligated to their respective vectors through Gibson assembly. After the obtained DNA was transformed into NEB10BETA competent cells (NEB) and miniprep, DNA sequencing showed the correct insertion of RagA, RagC and Ragulator genes in their respective vectors. Thereafter, the assembled plasmids were transformed into LOBSTR competent cells that were grown for large scale protein expression.

#### 4.1.2 Expression and purification of the core components

##### 4.1.2.1 RagA

The RagA construct, efficiently expressed in the LOBSTR *E. coli* strain, was at first purified by affinity chromatography. In order to increase the purity, the protein was not eluted but released from the resin through cleavage of its Hexa-histidine tag by a Glutathione S-transferase-tagged HRV3C protease.

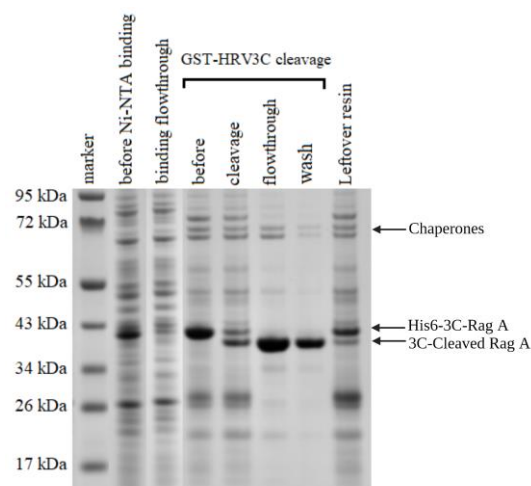


Figure 17: SDS-PAGE analysis of RagA's His-Affinity purification. Lysate samples were taken before and after binding to Ni-NTA resin. The HRV3C cleavage samples were taken directly on the resin bound-protein,

respectively after the last buffer wash (before), after the overnight incubation with the HRV3C protease (cleavage) and from the cleavage flowthrough and wash.

The RagA construct, appearing as the heavy bold band below 43 kDa, showed a high expression in bacteria, as it seems to be present in significant amounts in the cell lysate before Ni-NTA binding (Figure 17). The absence of that band in the binding flowthrough shows an efficient binding to the Ni-NTA resin. As mentioned above, the protein was not eluted but was instead released from the resin through overnight cleavage of its His-Tag by a HRV3C protease. The cleavage wasn't 100% efficient, as there appears to be quite a population of uncleaved RagA construct. It did enable to increase the purity of the final protein sample, releasing the cleaved construct along with its chaperone proteins. Only a small portion of which remained on the resin, along with the uncleaved construct (probably because it is attached to the chaperones). Releasing the protein through protease cleavage was successful as both the uncleaved construct and the Histidine-rich contaminants remained bound to the resin (Figure 17). The pulled cleavage flowthrough and wash, concentrated to a 4.6 mL volume gave a concentration of 117.02  $\mu$ M.

#### 4.1.2.2 RagC

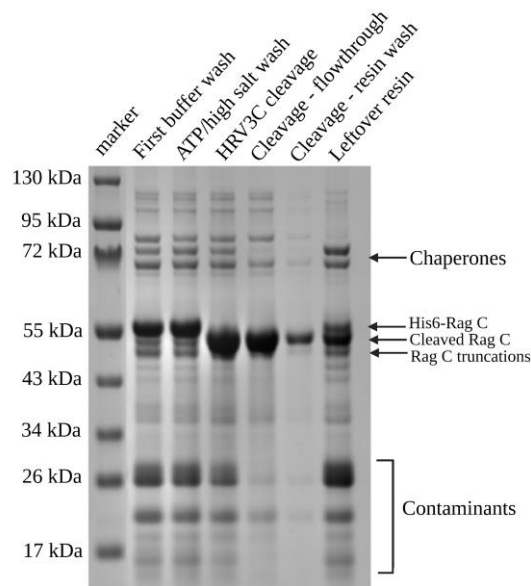


Figure 18: SDS-PAGE analysis of RagC's His-affinity purification. This gel shows the analysis of all the samples taken throughout the RagC's affinity purification, after each resin buffer wash and at each cleavage step, and finally from the leftover resin.

Similarly as for RagA, RagC was purified through Histidine-affinity chromatography. The ATP/high-salt buffer wash did not increase the overall purity and did not actually remove the chaperone proteins. The release of the protein by cleavage of its N-terminal His-Tag by a GST-tagged HRV3C protease, enabled to improve the purity of the final sample. RagC truncations are observed in Figure 18, especially in the washes and leftover resin samples. This could be due to partial digestion by proteases, and is a possible explanation for why the RagC construct band became smeary after cleavage, overlapping with the truncations bands. Thanks to a high cleavage efficiency, most of the cleaved construct was released from the resin in both the cleavage flowthrough and wash fractions. Only a small portion remained on the leftover resin. A few contaminants seem to remain in the final protein sample (Figure 18), but will be removed by size exclusion chromatography after the nucleotide exchange is performed. The pulled flowthrough and wash, concentrated to a 4 mL volume gave a concentration of 447.24  $\mu$ M.

#### 4.1.2.3 RagA – RagC dimer

Some issues faced with the GDP exchange of RagC, described later in this section, compromised the reconstitution of the RagA•GDP–RagC•GDP and RagA•GTP–RagC•GDP complexes with Ragulator. To counteract this issue and enable the reconstitution of the GDP-GDP complex, the wild type Rag GTPases were expressed as a dimer, with an hexa-histidine tag on RagC, for nucleotide exchange with GDP nucleotides.

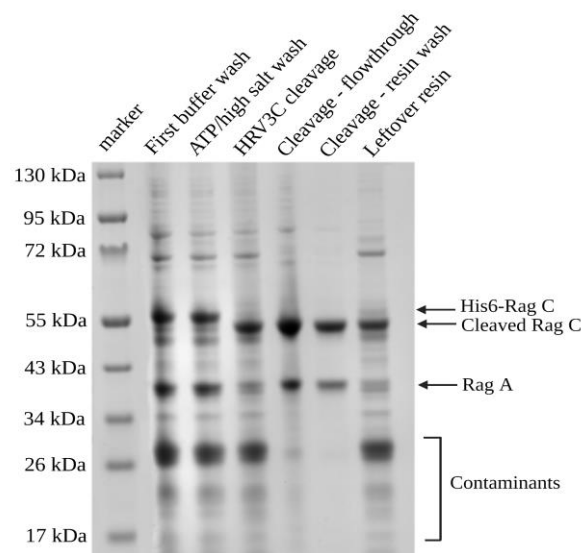


Figure 19: SDS-PAGE analysis of the His-affinity purification of the RagA–RagC dimer construct. This gel shows the analysis of all the samples taken throughout the Rags dimers' Ni-NTA purification.

The cleavage of RagC's hexa-histidine tag by HRV3C protease, enabled the Rags dimer to be released from the Ni-NTA resin after the buffer washes. Both RagA and RagC bands are observed in the cleavage flowthrough and wash fractions, though some cleaved RagC construct, in monomer, seems to have remained bound on the resin, along with most of the impurities and a very small proportion of RagA. (Figure 19) The pulled cleavage flowthrough and wash fractions, concentrated to a 1.5 mL volume gave a concentration of 460.76  $\mu$ M.

#### 4.1.2.4 Regulator

The pentameric complex Regulator, is the other core component of the Rag-Regulator complexes that are to be reconstituted. This complex consists of 5 different subunits : c7orf59, HBXIP, p14, MP1 and p18. Tags were attached to two of these subunits, along with the protease cleavage sites : an hexa-histidine tag and an HRV3C protease cleavage site on c7orf59 and a GST tag with a TEV protease cleavage site on p18. The complex was at first purified through GSH-affinity chromatography, both tags were cleaved off on GSH resin using His7-TEV and His6-HRV3C, and the purified complex was then incubated with Ni-NTA resin to remove cleaved tag and the proteases.

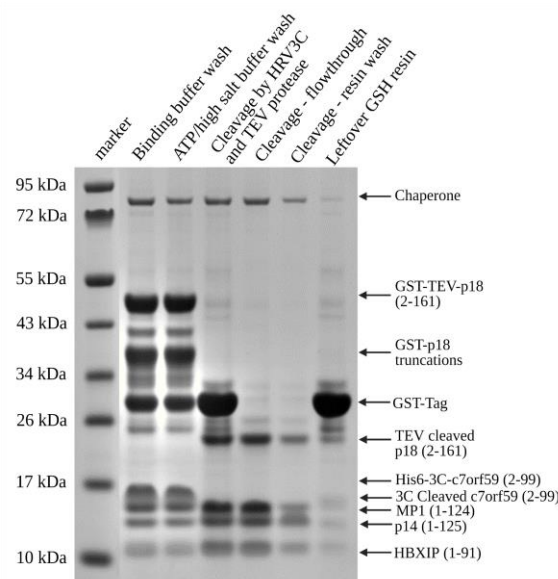


Figure 20: SDS-PAGE analysis of the Regulator complex's GSH-affinity purification. This gel shows the analysis of all the samples taken throughout this affinity purification.

The ATP/High-salt wash did not improve the overall purity before cleavage by proteases and

did not significantly affect the presence of the chaperone protein (Figure 20). Several bands are observed in the washes samples in Figure 20, between 55 kDa and 26 kDa. The obvious one is GST-p18 between 55 and 43 kDa, but there also appears to be some GST-p18 truncations between 43 and 30 kDa, along with some GST-Tag unbound to p18 above 26 kDa, which may be due to leaky expression. The cleavage of GST-p18 by the His7-TEV protease was close to a 100% efficient, as the GST-p18 band disappears and a size shift is observed from 44,5 kDa to distinctively ~24 kDa for p18, that runs above its real 17,7 kDa size, and ~27 kDa for GST (Figure 20). Similarly, a shift is observed on the c7orf59 subunit running below 17 kDa, after the cleavage of its hexa-histidine tag by the His6-HRV3C protease. This subunit runs above its 10,7 kDa size and forms the dome observed on the gel. The bands of p14 and MP1, of respectively 13,5 and 13,6 kDa, overlap on the gel. Finally the band corresponding to HBXIP, can be observed around 11 kDa, above its 9,6 kDa size. Both the binding to GSH resin and the release by tag cleavage enabled to get a sample with very little impurities. It also avoided GST tag sample pollution as it remained bound to the GSH resin, improving the chance to obtain a very pure sample after gel filtration. In order to remove the small number of remaining contaminants, along with the leftover tags and proteases, the cleavage flowthrough and wash fractions were pulled and incubated with His-affinity resin and later passed through a filter column.

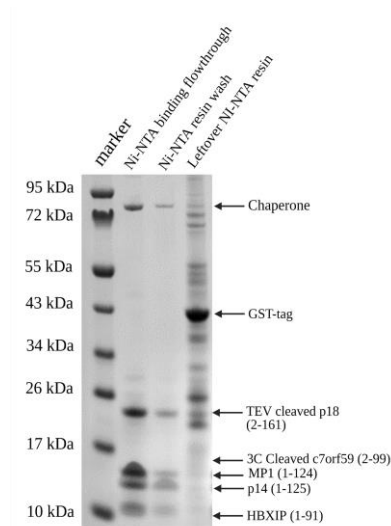


Figure 21: SDS-PAGE analysis of the Ragulator complex's Histidine-affinity purification. This gel shows the analysis of all the samples taken throughout Ragulator's His-affinity purification.

The binding flowthrough shows clean protein fractions of the 5 ragulator subunits : c7orf59, HBXIP, p14, MP1 and p18. It looks like some GST bound unspecifically to the Ni-NTA resin

(Figure 21), which enabled to get a very clean final sample before the gel filtration run. Only the large molecular weight chaperone remained present.

The Ragulator complex was then run on a Superdex200 16/600 size exclusion chromatography column to separate the full complex from the large molecular weight chaperones that didn't get off in the affinity chromatography step.

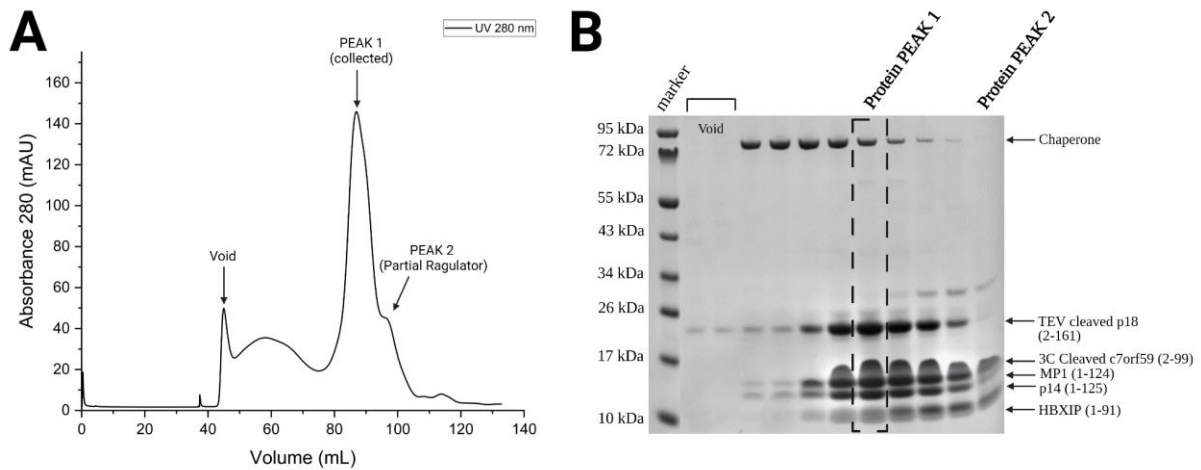


Figure 22: Size exclusion purification of the Pentameric Ragulator Complex. (A) Gel filtration chromatogram. (B) SDS-PAGE analysis.

Some chaperone still came out in the Ragulator peak, although most of it came out earlier during the run (Figure 22A,B). This could be a chaperone that plays an important role in maintaining the Ragulator complex, which could explain why it doesn't fully separate. There also appears to be some partially assembled Ragulator contamination in the second peak, where p18 appears to be degraded (Figure 22B). Nevertheless, the final sample is overall quite pure. The peak 1 containing fractions were pulled and concentrated giving a final concentration of 407.58  $\mu$ M in a 1.5 mL volume.

### 4.1.3 RagA•GppNHp – RagC•GppNHp – Ragulator

The aim is to image the Rag-Ragulator complex in one of its transient states, when both Rag GTPases are bound to GTP. Nevertheless, it is hard to predict which nucleotide bound state the purified Rag GTPases will be in at the point of imaging. Moreover, the GTP bound state is transient, as GTP is easily hydrolyzable. Therefore, RagA and RagC were exchanged with GppNHp, a non hydrolyzable GTP analog, enabling to lock the Rag GTPases in this specific

GTP bound conformation. The exchanged Rags were then run on size exclusion chromatography for purification and desalting before undergoing UPLC analysis to ensure the success of the exchange.

#### 4.1.3.1 Size exclusion purification of the GppNHp exchanged GTPases

Both constructs were run on size exclusion chromatography on a Superdex200 16/600 column to remove the excess nucleotides, along with potential impurities from the Ni-NTA purification.

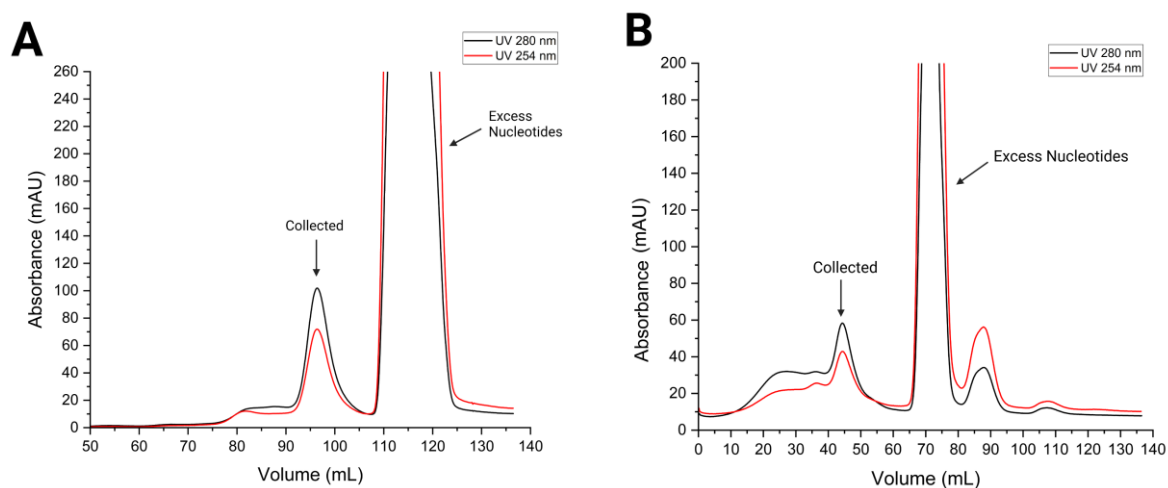


Figure 23: Size exclusion purification chromatograms of RagA and RagC after Nucleotide exchange, showing sample absorbance at 254 and 280 nm. (A) RagA - GppNHp. (B) RagC - GppNHp.

The size exclusion profiles showed the separation of the exchanged constructs from the excess nucleotides. RagA's purification resulted in a clean and sharp peak. (Figure 23A) The RagC construct shows a higher level of void aggregation and was eluted quite early in the run (Figure 23B), which is due to a mistake in the Äkta program that started the elution after 0 CV instead of 0.28 CV as for the RagA construct. Nevertheless, the purification was successful. The concentrated collected fractions of each construct gave a final concentration of 95.3  $\mu\text{M}$  in a 1 mL volume for RagA and 192.97  $\mu\text{M}$  in a 250  $\mu\text{L}$  volume for RagC.

### 4.1.3.2 UPLC Analysis

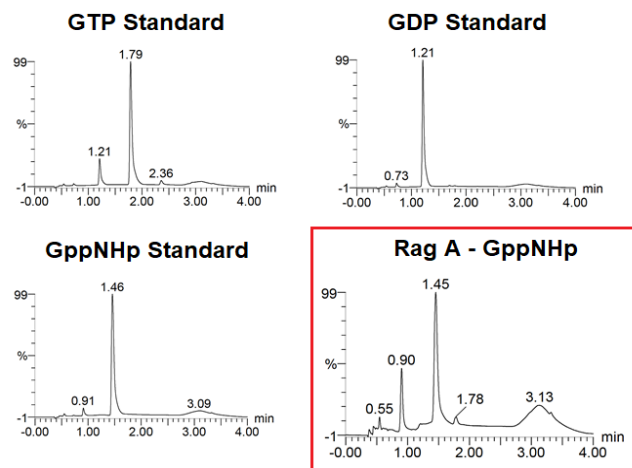


Figure 24: UPLC analysis of the nucleotide exchange of RagA with GppNHp nucleotides, along with the nucleotide standards of GDP, GTP and GppNHp showing the nucleotides absorbance at 254 nm in percentage.

The nucleotide standards of GppNHp, GTP and GDP were included in the UPLC analysis, enabling to compare the peaks with those obtained by the analysis of the GppNHp exchanged RagA. The peaks observed in the GTP and GDP nucleotides analysis, do not show in the RagA•GppNHp sample analysis (Figure 24). On the other hand, peaks are observed on both the GppNHp standard and the RagA•GppNHp sample around 0.90 min, 1.45 min and 3.10 minutes, with a 1 to 4 seconds difference. The exchange of RagA with GppNHp was thus successful.

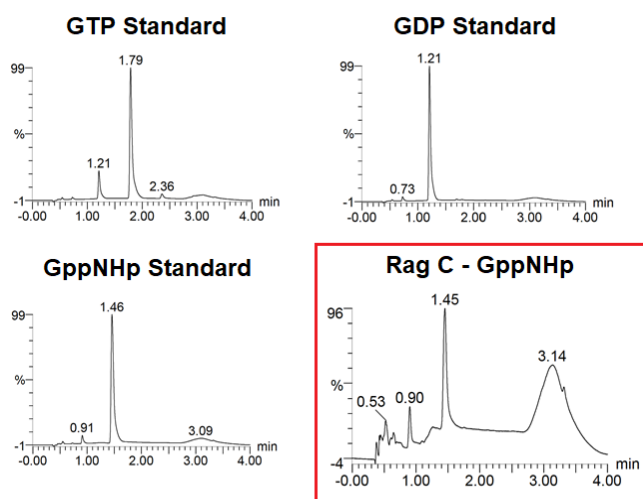


Figure 25: UPLC analysis of the nucleotide exchange of RagC with GppNHp nucleotides, along with the nucleotide standards of GDP, GTP and GppNHp, showing the nucleotides absorbance at 254 nm in percentage.

Similarly as for RagA, the purified RagC construct exchanged with GppNHp does not present the peaks observed for the GDP and GTP nucleotide standards, but presents peaks at the same time points as the GppNHp standard around 0.90 min, 1.45 min and 3.10 minutes with a 1 to 5 seconds difference (Figure 25). The exchange of RagC with GppNHp was thus successful.

#### 4.1.3.3 Reconstitution of the complex

As mentioned previously, the p18 subunit of Ragulator plays a big role in its interaction with the Rag GTPases and thus in the assembly and stability of the Rag-Ragulator complex along with p14 and MP1. Because of its N-terminal tail-like structure, p18 gets easily truncated by proteases. A too large concentration of degraded p18 in the complex reconstitution would compromise the assembly of the Rag-Ragulator complex, to the profit of a significant amount of the RagA–RagC heterodimer. To avoid this, the complex reconstitution reaction was set up with a stoichiometry of 1:1:3 (RagA : RagC : Ragulator), increasing the chances of a successful Rag-Ragulator complex assembly. The reconstituted complex was obtained after an overnight incubation and ran on size exclusion chromatography through injection onto a Superdex200 10/300 column.

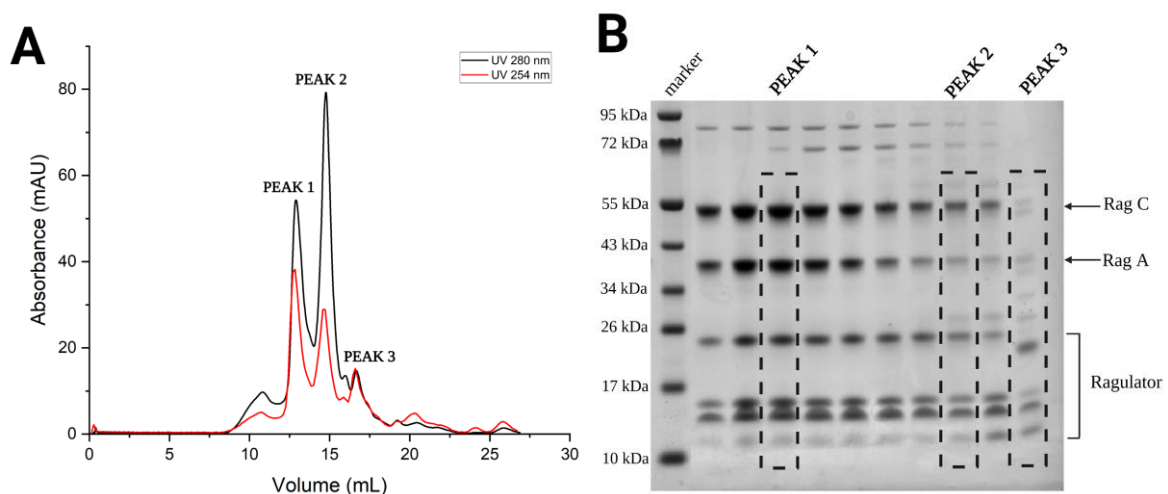


Figure 26: Size exclusion of the RagA•GppNHp–RagC•GppNHp–Ragulator complex reconstitution. (A) chromatogram, (B) SDS-PAGE analysis.

The different protein profiles were nicely separated by size exclusion chromatography. The fully reconstituted complex is eluted in the first peak, around 12.5 mL (Figure 26A). All the

complex components of the complex : RagA, RagC, and the 5 Ragulator subunits, appear in the SDS-PAGE analysis of this first protein profile, though the HBXIP subunit looks very shady (Figure 26B) which has also been observed in previous reconstitutions (Appendix 1). The second profile eluted around 15 mL also seems to contain the 5 Ragulator subunits as well as RagC, but RagA appears to be less present, which explains the size shift observed. In the third peak, eluted around 17 mL, both RagA and RagC appear to have been degraded. In addition to this, the Ragulator subunit p18, previously running right below 26 appears to be truncated, as a small size shift is observed between the peak 2 and peak 3 samples on the gel (Figure 26B). The concentrated peak 1 containing fractions gave a final concentration of 90.77  $\mu$ M, in a 50  $\mu$ L volume.

## 4.1.4 RagA•GDP – RagC•GppNHp – Ragulator

The RagC•GppNHp construct obtained from the exchange of RagC with GppNHp, and used in the previous reconstitution was here also used as a binding partner for RagA. Thus, the nucleotide exchange was only performed on RagA to obtain a GDP bound construct.

### 4.1.4.1 Nucleotide exchange of RagA with GDP

The sample resulting from the exchange of RagA with GDP was run on a Superdex 16/600 for size exclusion chromatography and a UPLC analysis was later performed to ensure that the construct was successfully loaded with GDP. The size exclusion chromatography of RagA•GDP gives a clean protein profile, nicely separated from the excess nucleotides (Figure 27B).

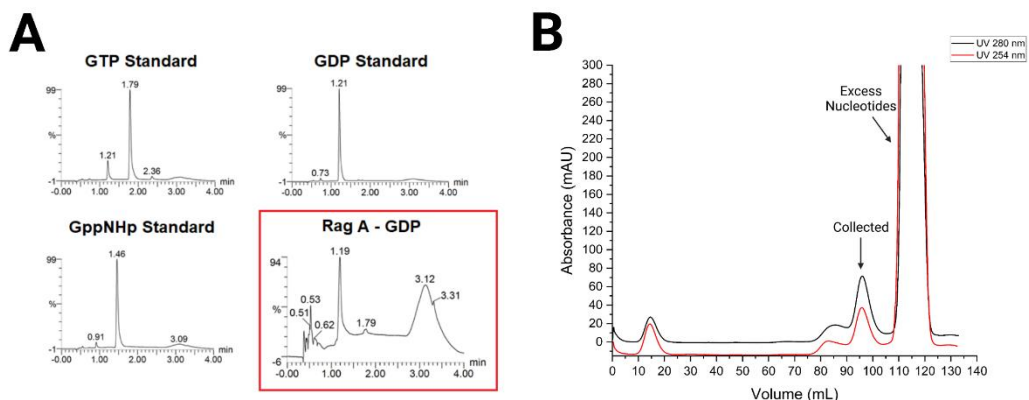


Figure 27: Nucleotide exchange of RagA with GDP. (A) UPLC chromatography analysis, showing the nucleotides absorbance at 254 nm in percentage (B) Size exclusion purification of the exchanged RagA•GDP, showing absorbance curves at 280 and 254 nm.

The UPLC analysis of GDP exchange on RagA (Figure 27A) appears to be quite strange. The GDP peak is clearly present at 1.19 minutes, but there seems to be a lot of “background” contamination, observed from the small peak at 1.79 minutes and the loopy peak at 3.12 minutes. This could be due to contaminations from the previous runs. RagA nevertheless appears to be loaded with GDP.

#### 4.1.4.2 Complex reconstitution

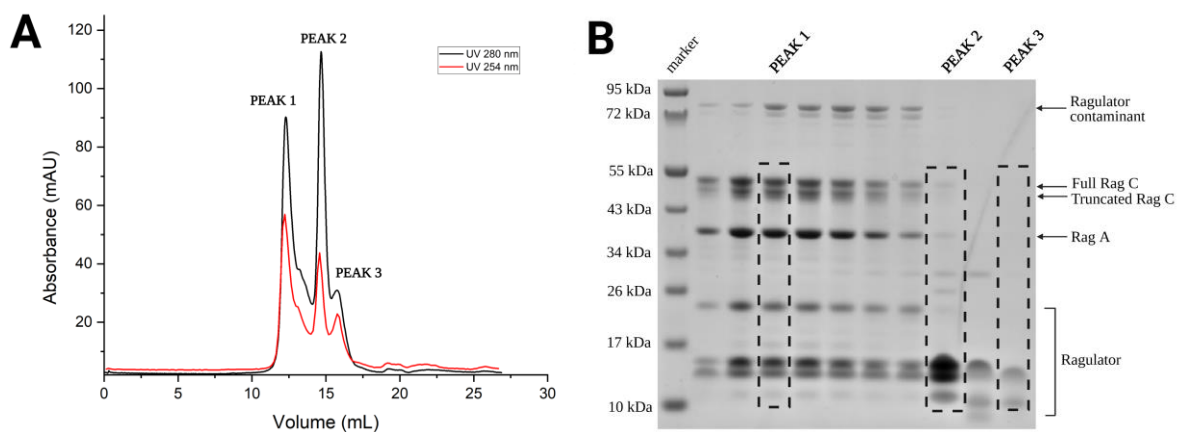


Figure 28: Size exclusion of the complex reconstitution (A) chromatogram, (B) SDS-PAGE analysis

As observed in the previous reconstitution, the fully reconstituted complex is eluted at 12.5 mL. The corresponding peak shown in the SDS-PAGE analysis contains all 7 proteins of the reconstituted complex : RagA•GDP, RagC•GppNHp, p18, p14, MP1, c7orf59 and HBXIP. Whereas only p14, MP1, c7orf59 and HBXIP are present in the second peak and the third peak contains almost no protein (Figure 28A,B). The concentrated peak 1 containing fractions gave a final concentration of 24.04  $\mu$ M, in a 30  $\mu$ L volume.

## 4.1.5 RagA•GDP – RagC•GDP – Ragulator

### 4.1.5.1 Nucleotide exchange of RagC with GDP

The RagA construct, previously exchanged with GDP nucleotides was to be used in this reconstitution as well. Thus, only RagC remained to be exchanged with GDP.

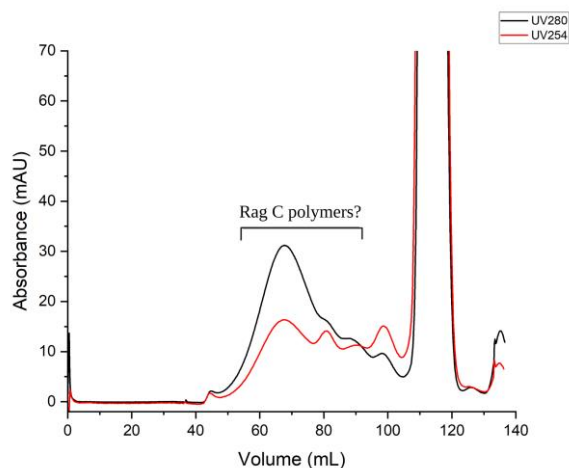


Figure 29: Size exclusion chromatogram of RagC after nucleotide exchange with GDP.

The size exclusion profile of the GDP exchanged RagC construct shows a nice separation of the protein from the excess GDP nucleotides. Nevertheless, there appears to some unexpected protein profiles : a large peak is eluted around 70 mL and other small peaks are observed around 80 mL, 90 mL and 100 mL (Figure 29) when it had been observed from previous protein preps that RagC is usually eluted between 85 mL and 90 mL on Superdex200 16/600 column.

This could be explained by a possible phenomenon of polymerization of RagC. It is unlikely to be aggregated, as very little protein is present in the void volume, eluted around 45 mL (Figure 29). Regardless, the uncertainty made this exchanged RagC useless for complex reconstitution for further structural studies. This compromised both the RagA•GDP–RagC•GDP–Ragulator and RagA•GTP–RagC•GDP–Ragulator reconstitutions. In order to skirt this issue, the Rag GTPases were exchanged with GDP as a dimer, aiming to perform the RagA•GDP–RagC•GDP–Ragulator reconstitution.

#### 4.1.5.2 Nucleotide exchange of the Rags dimer with GDP

Just like the RagA construct, the RagA–RagC dimer was exchanged with high quality GDP nucleotides in a 1:5 molar ratio of MgCl<sub>2</sub> and EDTA, supplemented with 50mM GluArg.

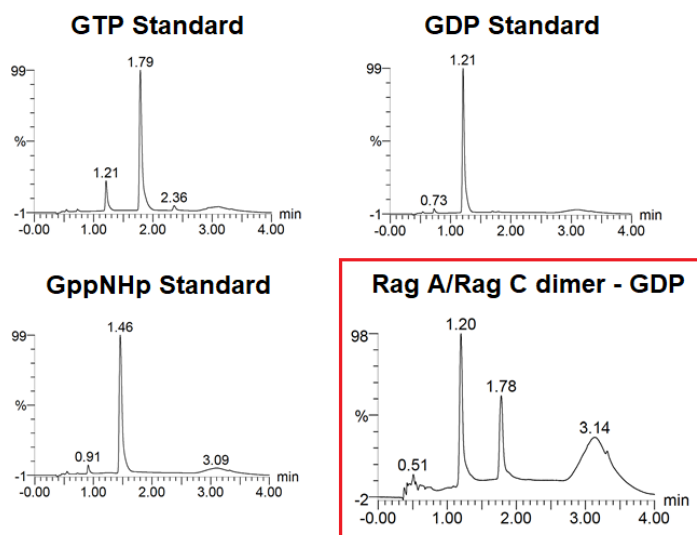


Figure 30: UPLC chromatography analysis of the Nucleotide exchange of the RagA-RagC dimer with GDP, showing the nucleotides absorbance at 254 nm in percentage.

The UPLC analysis of the GDP exchanged Rags dimer shows a sharp peak at 1.20 minutes, which can be identified in the GDP nucleotide standard, but also a sharp peak at 1.78 minutes that is identified in the GTP standard. In addition to this, the sample also presents a peak at 3.14 minutes, similarly as the one observed in the GppNHp standard, (Figure 30) which can be assimilated to a small GppNHp contamination of the column. Nevertheless, there seems to be a mixture of GTP and GDP bound RagA–RagC dimer, from which it can be concluded that the GDP exchange was unsuccessful. Despite several more trials, this compromised the reconstitution of the GDP-GDP complex.

## 4.2 Reconstitution of SLC38A9 in an NW11 nanodisc

### 4.2.1 Cloning, transformation, and sequencing of NW11

After the NW11 gene insert was amplified through PCR, inserted and ligated to the pFloat.T7 vector through Gibson Assembly, the DNA was transformed into NEB10BETA competent cells and miniprep. DNA sequencing showed the correct insertion of the gene into the vector. After what, the assemble plasmid was transformed into LOBSTR competent cells that were grown for large scale protein expression.

### 4.2.2 Expression and purification of NW11

The membrane scaffold protein NW11 construct was cloned with an Avi-Tag to later enable protein biotinylation and with a Cysteine-containing fusion tag for site targeted drug screening experiments. A deca-histidine tag was also added, along with a 3C protease cleavage site for His affinity purification.

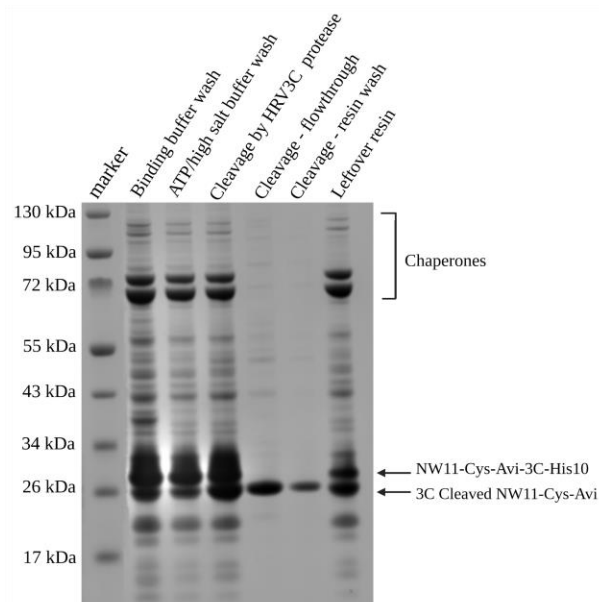


Figure 31: SDS-PAGE analysis of the His-Affinity purification of the NW11 construct

The NW11 construct showed a high expression in bacteria. The corresponding band, running right above 26 kDa appears quite smeary. This is especially observed in the washes and cleaved samples in Figure 31, and could be due to the high protein expression. There also

appears to be two NW11 populations, even before cleavage by HRV3C. The band running at the size of the cleaved construct could be a His-tagged NW11 truncation, as it's not coming off the resin during the washes. The later slightly improved the purity, but many of the impurities remained present. It is hard to evaluate the efficiency of the cleavage by HRV3C because of the presence of the NW11 truncation running at the same size, though the band right below 26 kDa seems to get thicker in the cleavage sample (Figure 31). Nevertheless, some cleavage did occur as the cleavage flowthrough and wash samples contain the cleaved construct with a very high purity. Nonetheless, a strong population of uncleaved construct is still present both in the cleavage sample and on the leftover resin. Thus, the NW11 bound to the leftover resin was again incubated at 4°C overnight with 1.2 μM HRVC protease for further cleavage.

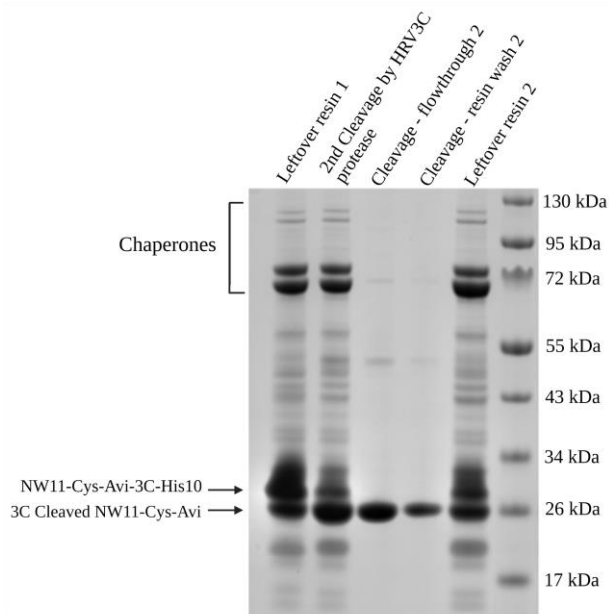


Figure 32: SDS-PAGE analysis of the Second incubation of the NW11 construct with HRV3C protease for further cleavage.

This second cleavage looks similar to the first one, though the band of the uncleaved NW11 construct gets weaker more significantly, while the band of the cleaved construct gets stronger. The cleaved construct is again released from the resin in the cleavage flowthrough and wash fractions. The two populations of NW11 are still present on the leftover resin (Figure 32), but a more significant amount got released compared to the first cleavage. Considering the level of sample purity, the flowthrough and wash fractions from both cleavages were pulled together, concentrated and flash frozen in LN<sub>2</sub> for later use in nanodisc reconstitution.

## 4.2.3 Expression and purification of SLC38A9

### 4.2.3.1 Affinity Purification

SLC38A9 is to be expressed with short glycans, to facilitate future drug screening experiments. This was done through treatment of the cells with Kifunensine. The protein was expressed with a Flag-tag, facilitating purification to obtain a very pure sample, as very few of the other proteins will be binding to the anti-flag resin.

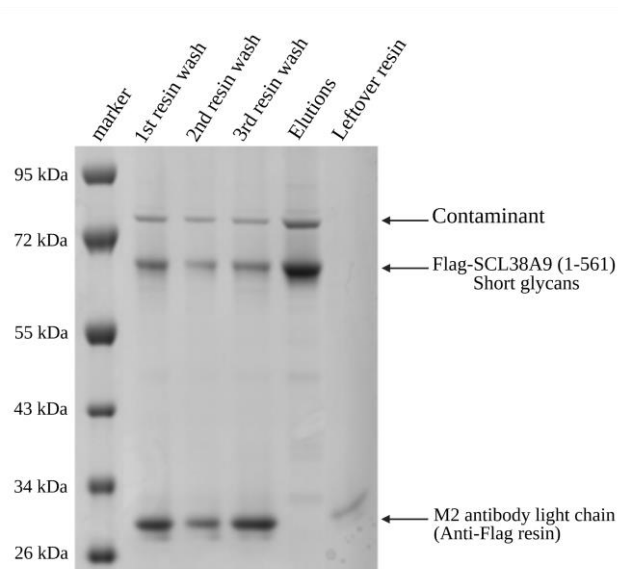


Figure 33: SDS-PAGE analysis of SLC38A9's Flag-purification

Elution from Anti-flag resin using a 3xFlag peptide indeed enabled to obtain an almost contaminant-free protein preparation, even before the buffer washes. The only contaminant that seems to remain and is eluted by the Flag-peptide addition is running right above 72 kDa (Figure 33). It could be a chaperone protein of SLC38A9, which would explain why it doesn't get separated by Flag-affinity purification. The fully glycosylated SLC38A9 tends to run as a large smear (52), the reason for this stretch is the length of the glycans and their heterogenous distribution. The expression with short glycans looks successful, as there seems to be a homogenous glycans distribution, resulting in the protein running as a clear band rather than a smear. The elution fractions were pulled and concentrated for size exclusion purification, enabling to assess the stability of SLC38A9 when expressed with short glycans.

### 4.2.3.2 Size exclusion purification

Even though the sample obtained after elution of SLC38A9 from flag resin was highly pure, a size exclusion chromatography step was performed both to remove the high molecular weight contaminant that remained after the Flag purification, and to assess protein stability after its expression with short glycans. This cannot be seen on SDS-PAGE as the protein is denatured. Thus, the concentrated protein sample was injected onto a Superdex 200 10/300 column for gel filtration purification.

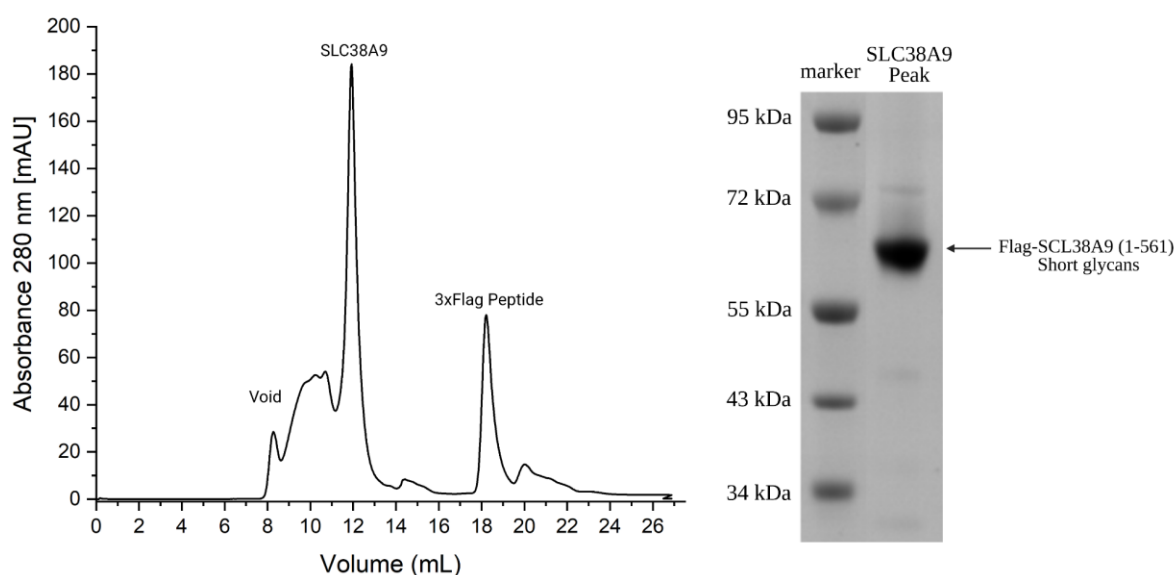


Figure 34: Size exclusion chromatogram of SLC38A9 showing the absorbance curve at 280 nm and SDS-PAGE analysis of the corresponding protein peak.

The size exclusion profile of the short glycans SLC38A9 shows a nice and sharp peak, which emphasizes a nice protein folding and stability (77). This step seems to have significantly removed the contaminant running above 72 kDa, though a small amount remains. (Figure 34) This is very promising for the next steps of the nanodisc reconstitution and later the drug screening experiments. The concentrated fractions of the SLC38A9 protein peak gave a final concentration of 17.82  $\mu$ M in a 240  $\mu$ L volume.

## 4.2.4 Determination of the lipid composition and ratio for nanodisc assembly

Different ratios and compositions of the lipids majoritarily present in biological membranes were used in order for the SLC38A9 in nanodisc to be as representative as possible to those found in Nature. This simultaneously enabled to assess the assembly, stability and separation of the reconstituted nanodiscs, both with and without SLC38A9 through size exclusion chromatography.

### 4.2.4.1 Empty nanodisc reconstitution trials

NW11 was incubated with different ratios of lipids for nanodisc reconstitution trials. The resulting samples were run on size exclusion chromatography on a superose 6 3.2/300 column.

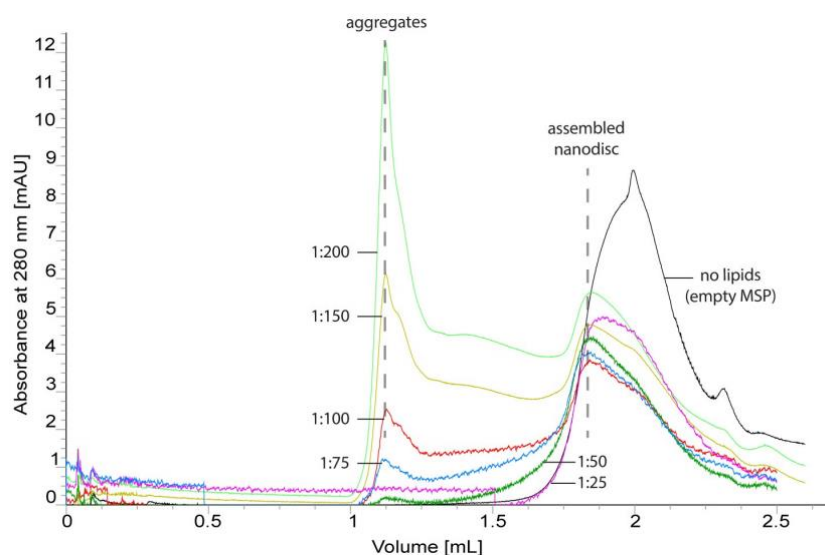


Figure 35: Overlay of size exclusion runs of nanodiscs reconstitution with NW11 and lipids (Phosphatidylcholine, phosphatidylethanolamine and cholesterol) at 6 different ratios : 1:25, 1:50, 1:75, 1:100, 1:150, and finally 1:200.

A small size shift is observed in Figure 35 between the empty NW11 (MSP) coming out around to 2.1 mL, and the NW11 loaded with lipids, coming out closer to 1.9 mL. This enables to evaluate the successful assembly of the nanodisc. The lipid ratios above 1:100 gave a lot of aggregates, as a significant amount of protein came out in the void volume. It is observed from the curves that the higher the lipid ratio, the higher the amount of aggregates

(Figure 35). In the case of the 1:150 and 1:200 ratios, the amount of aggregates is even higher than the amount of assembled nanodisc. This can easily be explained as the hydrophobic interactions increase with the amount of lipids, thus forming more aggregates. The ratios below 1:100 on the other hand give a nicer result. There seems to be very little aggregation in the 1:75 ratio, whereas the 1:50 and 1:25 ratios almost don't give any, while still exhibiting a successful nanodisc assembly (Figure 35).

#### 4.2.4.2 Reconstitution trials of the nanodisc with SLC38A9 inside

After the reconstitution trials with NW11 alone, the NW11:lipid ratios 1:25, 1:50 and 1:75 were favored for reconstitution with SLC38A9, as they gave a nice separation and a very low amount of aggregates. SLC38A9 was added at a 1:10 ratio with NW11. Two lipid compositions were tried :

- Phosphatidylethanolamine (POPE), Phosphatidylcholine (POPC), Cholesterol (CHS)
- Phosphatidylethanolamine (POPE), Phosphatidylcholine (POPC), Cholesterol (CHS), Sphingomyelin (SM)

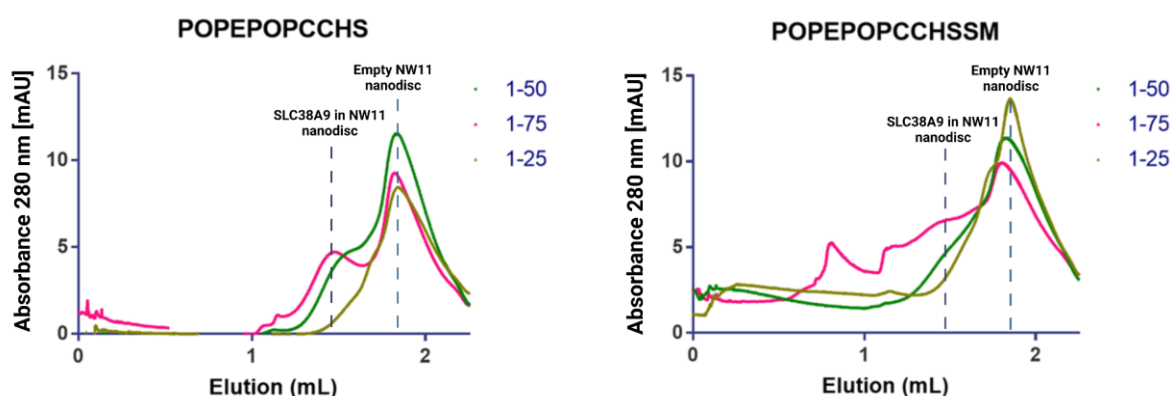


Figure 36: Overlay of size exclusion runs of nanodisc assembly trials with NW11 and SLC38A9, with different ratios of NW11 and Lipids (1:25, 1:50 and 1:75) and different lipid compositions of phosphatidylcholine, phosphatidylethanolamine, cholesterol and Sphingomyelin.

Once again, the successful assembly of the nanodisc with SLC38A9 inside is evaluated based on the size shift observed : the nanodisc containing SLC38A9 is eluted slightly before 1.5 mL, while the empty nanodisc with NW11 and lipids is eluted closer to 2 mL (Figure 36). The reconstitution without Sphingomyelin seems to result in a nicer assembly and incorporation of SLC38A9 into the nanodisc. The peak is sharper with the 1:75 ratio, which shows a more efficient entry of SLC38A9, while the ratio 1:50 results in a less sharp peak

and a stronger overlap with the empty NW11 nanodisc peak. The 1:25 ratio, doesn't seem to be enough for SLC38A9 to enter the nanodisc, as only the empty nanodisc peak is observed, while the peak around 1.5 mL is not (Figure 36). The presence of Sphingomyelin seems to complicate the incorporation of SLC38A9 into the nanodisc. Indeed, the peak around 1.5mL is not present for any of the tried lipid ratios, only the empty nanodisc peak is observed for all three. It thus seems like the ratio 1:75 is the one that would give the best full nanodisc assembly. Nevertheless, the successful incorporation of SLC38A9 will have to be evaluated by SDS-PAGE analysis, after the protocol scale-up.

## 4.2.5 Reconstitution of SLC38A9 into NW11 nanodiscs

The membrane protein SLC38A9 was reconstituted into the NW11 nanodisc in the following ratio 1:10:750 (SLC38A9 : NW11 : Lipids).

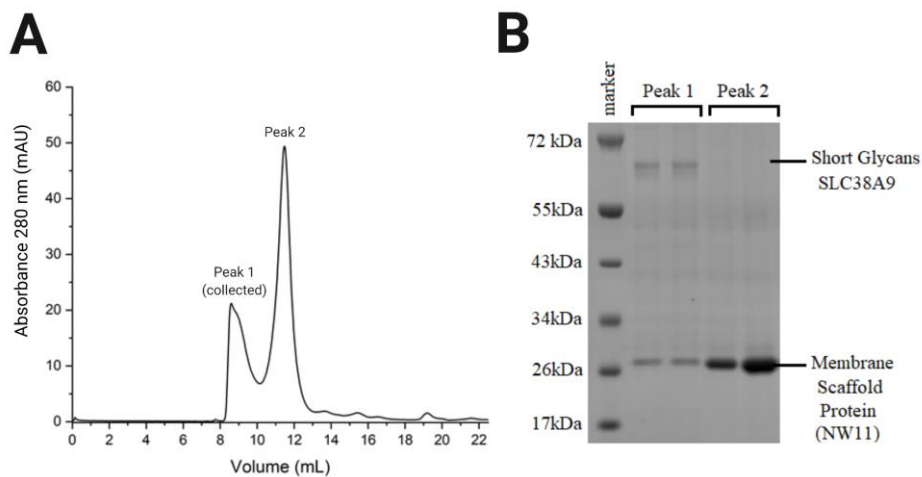


Figure 37: Size exclusion chromatography of the nanodisc reconstitution with SLC38A9 inside. (A) size exclusion chromatogram. (B) SDS-PAGE analysis.

The analysis of the protein profiles resulting from the size exclusion chromatography (Figure 37A), shows that the first eluted peak contains both SLC38A9 (expressed with short glycans) and the membrane scaffold protein NW11 whereas the secondly eluted profile contains NW11 alone (Figure 37B). It appears that SLC38A9 was fully incorporated in the nanodisc, as it doesn't show alone in any of the protein profiles. More interestingly, it looks from the gel in Figure 37B, that SLC38A9 and NW11 are present in the fully assembled nanodisc at a close to 1:1 ratio which would imply that each NW11 molecule is loaded with one SLC38A9. This implies that all the excess NW11 is eluted in the second peak, which is confirmed by SDS-gel observation.

## 5 Conclusions and Future directions

The two main focuses of the Master project were the reconstitution of the Rag-Ragulator complex in its 4 nucleotide-binding states, and the assembly of the membrane protein and amino acid transporter SLC38A9 in a membrane protein nanodisc, both involved in the activation of mTORC1 in response to amino acids.

The reconstitution of the RagA•GDP–RagC•GTP–Ragulator and RagA•GTP–RagC•GTP–Ragulator (using a non hydrolyzable GTP analog), is the first step for further investigating the conformational changes induced within the heterodimer, by the change in nucleotide-binding state. This would provide more knowledge on the GTPases mechanisms, but also more structural insight on how the Rag GTPases “open” and “close” the door of Raptor’s binding in the RagA•GTP–RagC•GDP conformation.

The reconstitution of the two remaining conformations, RagA•GTP–RagC•GDP–Ragulator, and RagA•GDP–RagC•GDP–Ragulator, was highly compromised by the challenges faced with the GDP exchange of both RagC and the GTPases heterodimer. In future trials, the GTPase-activating protein activity of GATOR1 might be used on a GTP exchanged Rags, to hydrolyse the GTP nucleotide bound to RagA, thus enabling the RagC-bound GTP to be hydrolyzed into GDP by the GAP activity of the FLCN-FNIP2 complex.

The reconstituted complexes are later to be imaged through Cryo-Electron microscopy for detailed structural studies, aiming to obtain structures of each of the four nucleotide-bound conformations.

The amino acid sensor and transporter SLC38A9, involved in pancreatic cancer cell growth, was produced in mammalian cells, treated with Kifunensine, which enabled the protein to be generated with short glycans. The purification of SLC38A9 through flag-affinity chromatography enabled to obtain a very pure protein sample to be used in nanodisc reconstitution. The Phosphatidylcholine : Phosphatidylethanolamine : Cholesterol lipid composition was favored over the one with added Shingomyelin, as it seemed like the presence of the later prevented the incorporation of SLC38A9 into the nanodisc. A possible explanation for this might be that the presence of Shingomyelin tightens the lipid rafts,

making it more difficult for SLC38A9 to incorporate into the nanodisc. Nevertheless, the reconstitution in a 1:10:750 ratio of SLC38A9, NW11 (MSP) and lipids resulted in a successful nanodisc assembly and SLC38A9 incorporation.

In order to increase the expression of SLC38A9, while generating it with short glycans, a new stable line for expression is to be generated in Expi GnT1- cells. These cells will lack N-acetylglucosaminyltransferase I (GnTI) activity and will therefore lack complex N-glycans. The next steps should be the selection of potential binders from a yeast nanobody library. Ultimately, the protein on nanodisc is to be imaged using Cryo-Electron Microscopy.

## 6 References

1. Saxton RA, Sabatini DM. mTOR Signaling in Growth, Metabolism, and Disease. *Cell*. 2017;168(6):960–76.
2. Chung J, Kuo CJ, Crabtree GR, Blenis J. Rapamycin-FKBP specifically blocks growth-dependent activation of and signaling by the 70 kd S6 protein kinases. *Cell*. 1992 Jun 26;69(7):1227–36.
3. Sabers CJ, Martin MM, Brunn GJ, Williams JM, Dumont FJ, Wiederrecht G, et al. Isolation of a protein target of the FKBP12-rapamycin complex in mammalian cells. *J Biol Chem*. 1995 Jan 13;270(2):815–22.
4. Guertin DA, Sabatini DM. An expanding role for mTOR in cancer. *Trends Mol Med*. 2005 Aug;11(8):353–61.
5. Kim DH, Sarbassov DD, Ali SM, King JE, Latek RR, Erdjument-Bromage H, et al. mTOR interacts with raptor to form a nutrient-sensitive complex that signals to the cell growth machinery. *Cell*. 2002 Jul 26;110(2):163–75.
6. Yang H, Jiang X, Li B, Yang HJ, Miller M, Yang A, et al. Mechanisms of mTORC1 activation by RHEB and inhibition by PRAS40. *Nature*. 2017;552(7685):368–73.
7. Guertin DA, Stevens DM, Thoreen CC, Burds AA, Kalaany NY, Moffat J, et al. Ablation in mice of the mTORC components raptor, rictor, or mLST8 reveals that mTORC2 is required for signaling to Akt-FOXO and PKCalpha, but not S6K1. *Dev Cell*. 2006 Dec;11(6):859–71.
8. Ben-Sahra I, Manning BD. mTORC1 signaling and the metabolic control of cell growth.
9. Inoki K, Li Y, Xu T, Guan KL. Rheb GTPase is a direct target of TSC2 GAP activity and regulates mTOR signaling. *Genes Dev*. 2003 Aug 1;17(15):1829–34.
10. Gwinn DM, Shackelford DB, Egan DF, Mihaylova MM, Mery A, Vasquez DS, et al. AMPK phosphorylation of raptor mediates a metabolic checkpoint. *Mol Cell*. 2008 Apr 25;30(2):214–26.
11. Inoki K, Zhu T, Guan KL. TSC2 mediates cellular energy response to control cell growth and survival. *Cell*. 2003 Nov 26;115(5):577–90.
12. Brugarolas J, Lei K, Hurley RL, Manning BD, Reiling JH, Hafen E, et al. Regulation of mTOR function in response to hypoxia by REDD1 and the TSC1/TSC2 tumor suppressor complex. *Genes Dev*. 2004 Dec 1;18(23):2893–904.
13. Feng Z, Hu W, de Stanchina E, Teresky AK, Jin S, Lowe S, et al. The regulation of AMPK beta1, TSC2, and PTEN expression by p53: stress, cell and tissue specificity, and the role of these gene products in modulating the IGF-1-AKT-mTOR pathways. *Cancer Res*. 2007 Apr 1;67(7):3043–53.
14. Kim E, Guan KL. RAG GTPases in nutrient-mediated TOR signaling pathway. *Cell Cycle*. 2009 Apr 1;8(7):1014–8.
15. Chantranupong L, Wolfson RL, Orozco JM, Saxton RA, Scaria SM, Bar-Peled L, et al. The Sestrins Interact with GATOR2 to Negatively Regulate the Amino-Acid-Sensing Pathway Upstream of mTORC1. *Cell Reports*. 2014 Oct 9;9(1):1–8.
16. Gai Z, Wang Q, Yang C, Wang L, Deng W, Wu G. Structural mechanism for the arginine sensing and regulation of CASTOR1 in the mTORC1 signaling pathway. *Cell Discov*. 2016;2:16051.

17. Carroll B, Maetzel D, Maddocks OD, Otten G, Ratcliff M, Smith GR, et al. Control of TSC2-Rheb signaling axis by arginine regulates mTORC1 activity. *Elife*. 2016 Jan 7;5.
18. Holz MK, Ballif BA, Gygi SP, Blenis J. mTOR and S6K1 mediate assembly of the translation preinitiation complex through dynamic protein interchange and ordered phosphorylation events. *Cell*. 2005 Nov 18;123(4):569–80.
19. Gingras AC, Gygi SP, Raught B, Polakiewicz RD, Abraham RT, Hoekstra MF, et al. Regulation of 4E-BP1 phosphorylation: a novel two-step mechanism [Internet]. 1999. Available from: [www.genesdev.org](http://www.genesdev.org)
20. Bar-Peled L, Sabatini DM. SnapShot: mTORC1 signaling at the lysosomal surface. *Cell*. 2012 Dec 7;151(6):1390-1390.e1.
21. Porstmann T, Santos CR, Griffiths B, Cully M, Wu M, Leever S, et al. SREBP activity is regulated by mTORC1 and contributes to Akt-dependent cell growth. *Cell Metab*. 2008 Sep;8(3):224–36.
22. Düvel K, Yecies JL, Menon S, Raman P, Lipovsky AI, Souza AL, et al. Activation of a metabolic gene regulatory network downstream of mTOR complex 1. *Mol Cell*. 2010 Jul 30;39(2):171–83.
23. Kim J, Kundu M, Viollet B, Guan KL. AMPK and mTOR regulate autophagy through direct phosphorylation of Ulk1. *Nat Cell Biol*. 2011 Feb;13(2):132–41.
24. Rebsamen M, Superti-Furga G. SLC38A9: A lysosomal amino acid transporter at the core of the amino acid-sensing machinery that controls MTORC1. *AUTOPHAGY* [Internet]. 2016;12(6):1061–2. Available from: <http://dx.doi.org/10.1080/15548627.2015.1091143>
25. Rebsamen M, Pochini L, Stasyk T, G de Araújo ME, Galluccio M, Kandasamy RK, et al. SLC38A9 is a component of the lysosomal amino acid-sensing machinery that controls mTORC1 Europe PMC Funders Group. *Nature* [Internet]. 2015;519(7544):477–81. Available from: [http://www.nature.com/authors/editorial\\_policies/license.html#terms](http://www.nature.com/authors/editorial_policies/license.html#terms)
26. Sancak Y, Bar-Peled L, Zoncu R, Markhard AL, Nada S, Sabatini DM. Ragulator-Rag complex targets mTORC1 to the lysosomal surface and is necessary for its activation by amino acids. *Cell*. 2010 Apr 16;141(2):290–303.
27. Mu Z, Wang L, Deng W, Wang J, Wu G. Structural insight into the Ragulator complex which anchors mTORC1 to the lysosomal membrane. *Nature Publishing Group* [Internet]. 2017;3. Available from: [www.nature.com/celldisc](http://www.nature.com/celldisc)
28. Zhang T, Wang R, Wang Z, Wang X, Wang F, Ding J. Structural basis for Ragulator functioning as a scaffold in membrane-anchoring of Rag GTPases and mTORC1. *Nature Communications*. 2017 Dec 1;8(1).
29. Liu Y, Cao J, Sun Y, Wai Fhu C, Ali A. Protein Lipidation by Palmitoylation and Myristoylation in Cancer. 2021; Available from: [www.frontiersin.org](http://www.frontiersin.org)
30. Nada S, Hondo A, Kasai A, Koike M, Saito K, Uchiyama Y, et al. The novel lipid raft adaptor p18 controls endosome dynamics by anchoring the MEK-ERK pathway to late endosomes. *EMBO J*. 2009 Mar 4;28(5):477–89.
31. Bar-Peled L, Schweitzer LD, Zoncu R, Sabatini DM. Ragulator is a GEF for the rag GTPases that signal amino acid levels to mTORC1. *Cell*. 2012 Sep 14;150(6):1196–208.
32. Abu-Remaileh M, Wyant GA, Kim C, Laqtom NN, Abbasi M, Chan SH, et al. Lysosomal metabolomics reveals V-ATPase and mTOR-dependent regulation of amino acid efflux from lysosomes.

33. Groenewoud MJ, Zwartkruis FJT. Rheb and Rags come together at the lysosome to activate mTORC1. *Biochem Soc Trans.* 2013 Aug;41(4):951–5.
34. Johnson DS, Chen YH. Ras family of small GTPases in immunity and inflammation. *Curr Opin Pharmacol.* 2012 Aug;12(4):458–63.
35. Song S, Cong W, Zhou S, Shi Y, Dai W, Zhang H, et al. Small GTPases: Structure, biological function and its interaction with nanoparticles. Vol. 14, *Asian Journal of Pharmaceutical Sciences.* Shenyang Pharmaceutical University; 2019. p. 30–9.
36. Cherfils J, Zeghouf M. Regulation of small GTPases by GEFs, GAPs, and GDIs. *Physiol Rev.* 2013 Jan;93(1):269–309.
37. Nicastro R, Sardu A, Panchaud N, de Virgilio C. biomolecules The Architecture of the Rag GTPase Signaling Network. Available from: [www.mdpi.com/journal/biomolecules](http://www.mdpi.com/journal/biomolecules)
38. Yonehara R, Nada S, Nakai T, Nakai M, Kitamura A, Ogawa A, et al. Structural basis for the assembly of the Regulator-Rag GTPase complex. *Nat Commun.* 2017;8(1):1625.
39. Shutes A, Phillips RA, Corrie JET, Webb MR. Role of magnesium in nucleotide exchange on the small G protein rac investigated using novel fluorescent Guanine nucleotide analogues. *Biochemistry.* 2002 Mar 19;41(11):3828–35.
40. Shen K, Choe A, Sabatini DM. Intersubunit Crosstalk in the Rag GTPase Heterodimer Enables mTORC1 to Respond Rapidly to Amino Acid Availability. *Molecular Cell.* 2017 Nov 2;68(3):552-565.e8.
41. Egri SB, Shen K. An interdomain hydrogen bond in the Rag GTPases maintains stable mTORC1 signaling in sensing amino acids. *Journal of Biological Chemistry.* 2021 Jul 1;297(1):100861.
42. Wittinghofer A, Vetter IR. Structure-function relationships of the G domain, a canonical switch motif. *Annu Rev Biochem.* 2011;80:943–71.
43. Hall BE, Bar-Sagi D, Nassar N. The structural basis for the transition from Ras-GTP to Ras-GDP. *Proc Natl Acad Sci U S A.* 2002 Sep 17;99(19):12138–42.
44. Conceptualization REL, Investigation RZ, Resources CYL. Structural Mechanism of a Rag GTPase Activation Checkpoint by the Lysosomal Folliculin Complex HHS Public Access.
45. Tsun ZY, Bar-Peled L, Chantranupong L, Zoncu R, Wang T, Kim C, et al. The folliculin tumor suppressor is a GAP for the RagC/D GTPases that signal amino acid levels to mTORC1. *Mol Cell.* 2013 Nov 21;52(4):495–505.
46. Bar-Peled L, Chantranupong L, Cherniack AD, Chen WW, Ottina KA, Grabiner BC, et al. A tumor suppressor complex with GAP activity for the Rag GTPases that signal amino acid sufficiency to mTORC1.
47. Sancak Y, Peterson TR, Shaul YD, Lindquist RA, Thoreen CC, Bar-Peled L, et al. The Rag GTPases bind raptor and mediate amino acid signaling to mTORC1. *Science.* 2008 Jun 13;320(5882):1496–501.
48. Jeong JH, Lee KH, Kim YM, Kim DH, Oh BH, Kim YG. Crystal Structure of the Gtr1pGTP-Gtr2pGDP Protein Complex Reveals Large Structural Rearrangements Triggered by GTP-to-GDP Conversion. *Journal of Biological Chemistry.* 2012 Aug 24;287(35):29648–53.
49. Pasqualato S, Renault L, Cherfils J. Arf, Arl, Arp and Sar proteins: a family of GTP-binding proteins with a structural device for “front-back” communication. *EMBO Rep.* 2002 Nov;3(11):1035–41.
50. Lei HT, Mu X, Hattne J, Gonen T. A conformational change in the N terminus of SLC38A9 signals mTORC1 activation. *Structure.* 2021;29(5):426-432.e8.

51. Wyant GA, Abu-Remaileh M, Wolfson RL, Chen WW, Freinkman E, Danai L v, et al. mTORC1 Activator SLC38A9 Is Required to Efflux Essential Amino Acids from Lysosomes and Use Protein as a Nutrient. *Cell* [Internet]. 2017 Oct 19;171(3):642-654.e12. Available from: <http://www.ncbi.nlm.nih.gov/pubmed/29053970>
52. Wang S, Tsun ZY, Wolfson RL, Shen K, Wyant GA, Plovanich ME, et al. Metabolism. Lysosomal amino acid transporter SLC38A9 signals arginine sufficiency to mTORC1. *Science*. 2015 Jan 9;347(6218):188–94.
53. Kimball SR, Gordon BS, Moyer JE, Dennis MD, Jefferson LS. Leucine induced dephosphorylation of Sestrin2 promotes mTORC1 activation. *Cell Signal*. 2016;28(8):896–906.
54. Chantranupong L, Scaria SM, Saxton RA, Gygi MP, Shen K, Wyant GA, et al. The CASTOR Proteins Are Arginine Sensors for the mTORC1 Pathway. *Cell*. 2016 Mar 24;165(1):153–64.
55. Shen K, Rogala KB, Chou HT, Huang RK, Yu Z, Sabatini DM. Cryo-EM Structure of the Human FLCN-FNIP2-Rag-Ragulator Complex. *Cell*. 2019 Nov 27;179(6):1319-1329.e8.
56. Petit CS, Roczniak-Ferguson A, Ferguson SM. Recruitment of folliculin to lysosomes supports the amino acid-dependent activation of Rag GTPases. *J Cell Biol* [Internet]. 2013 Sep 30;202(7):1107–22. Available from: <http://www.ncbi.nlm.nih.gov/pubmed/24081491>
57. Fromm SA, Lawrence RE, Hurley JH, Struct Mol Biol Author manuscript N. Structural mechanism for amino acid-dependent Rag GTPase nucleotide state switching by SLC38A9 HHS Public Access Author manuscript. *Nat Struct Mol Biol* [Internet]. 2020;27(11):1017–23. Available from: [http://www.nature.com/authors/editorial\\_policies/license.html#terms](http://www.nature.com/authors/editorial_policies/license.html#terms)
58. Iriana S, Ahmed S, Gong J, Annamalai AA, Tuli R, Hendifar AE. Targeting mTOR in Pancreatic Ductal Adenocarcinoma. *Frontiers in Oncology* [Internet]. 2016 Apr 25;6:99. Available from: <http://journal.frontiersin.org/Article/10.3389/fonc.2016.00099/abstract>
59. Ryan DP, Hong TS, Bardeesy N. Pancreatic adenocarcinoma. *N Engl J Med*. 2014 Sep 11;371(11):1039–49.
60. Neoptolemos JP, Kleeff J, Michl P, Costello E, Greenhalf W, Palmer DH. Therapeutic developments in pancreatic cancer: current and future perspectives. *Nat Rev Gastroenterol Hepatol*. 2018;15(6):333–48.
61. Utomo WK, Narayanan V, Biermann K, van Eijck CHJ, Bruno MJ, Peppelenbosch MP, et al. mTOR is a promising therapeutical target in a subpopulation of pancreatic adenocarcinoma. *Cancer Lett*. 2014 May 1;346(2):309–17.
62. Hassan Z, Schneeweis C, Wirth M, Veltkamp C, Dantes Z, Feurecker B, et al. MTOR inhibitor-based combination therapies for pancreatic cancer. *Br J Cancer*. 2018;118(3):366–77.
63. Xu R, Yang J, Ren B, Wang H, Yang G, Chen Y, et al. Reprogramming of Amino Acid Metabolism in Pancreatic Cancer: Recent Advances and Therapeutic Strategies. *Frontiers in Oncology* [Internet]. 2020 Sep 29;10:572722. Available from: <https://www.frontiersin.org/article/10.3389/fonc.2020.572722/full>
64. Mann KM, Ying H, Juan J, Jenkins NA, Copeland NG. KRAS-related proteins in pancreatic cancer. *Pharmacol Ther*. 2016;168:29–42.
65. Liu J, Ji S, Liang C, Qin Y, Jin K, Liang D, et al. Critical role of oncogenic KRAS in pancreatic cancer (Review). *Mol Med Rep*. 2016 Jun;13(6):4943–9.

66. Commisso C, Davidson SM, Soydaner-Azeloglu RG, Parker SJ, Kamphorst JJ, Hackett S, et al. Macropinocytosis of protein is an amino acid supply route in Ras-transformed cells. *Nature*. 2013 May 30;497(7451):633–7.
67. Bar-Sagi D, Feramisco JR. Induction of membrane ruffling and fluid-phase pinocytosis in quiescent fibroblasts by ras proteins. *Science*. 1986 Sep 5;233(4768):1061–8.
68. Doherty GJ, McMahon HT. Mechanisms of endocytosis. *Annu Rev Biochem*. 2009;78:857–902.
69. Amyere M, Payraastre B, Krause U, van der Smissen P, Veithen A, Courtoy PJ. Constitutive Macropinocytosis in Oncogene-transformed Fibroblasts Depends on Sequential Permanent Activation of Phosphoinositide 3-Kinase and Phospholipase C. Vol. 11, *Molecular Biology of the Cell*. 2000.
70. Yang JS, Wang CC, Qiu JD, Ren B, You L. Arginine metabolism: a potential target in pancreatic cancer therapy. 2020; Available from: [www.cmj.org](http://www.cmj.org)
71. Gibson DG. Enzymatic assembly of overlapping DNA fragments. *Methods Enzymol*. 2011;498:349–61.
72. Andersen KR, Leksa NC, Schwartz TU. Optimized E. coli expression strain LOBSTR eliminates common contaminants from His-tag purification. *Proteins: Structure, Function and Bioinformatics*. 2013 Nov;81(11):1857–61.
73. Brandi A, Pon CL. Expression of Escherichia coli cspA during early exponential growth at 37 °C. *Gene*. 2012 Jan 25;492(2):382–8.
74. Rosano GL, Ceccarelli EA. Recombinant protein expression in Escherichia coli: advances and challenges. *Front Microbiol*. 2014;5:172.
75. Studier FW, Moffatt BA. Use of bacteriophage T7 RNA polymerase to direct selective high-level expression of cloned genes. *J Mol Biol*. 1986 May 5;189(1):113–30.
76. Morales ES, Parcerisa IL, Ceccarelli EA. A novel method for removing contaminant Hsp70 molecular chaperones from recombinant proteins. *Protein Sci*. 2019;28(4):800–7.
77. Hong P, Koza S, Bouvier ESP. Size-Exclusion Chromatography for the Analysis of Protein Biotherapeutics and their Aggregates. *J Liq Chromatogr Relat Technol*. 2012 Nov;35(20):2923–50.
78. Errasti-Murugarren E, Bartoccioni P, Palacín M. Membrane Protein Stabilization Strategies for Structural and Functional Studies. *Membranes (Basel)*. 2021 Feb 22;11(2).
79. Denisov IG, Sligar SG. Nanodiscs for structural and functional studies of membrane proteins. *Nat Struct Mol Biol*. 2016 Jun;23(6):481–6.
80. Backer M v, Levashova Z, Levenson R, Blankenberg FG, Backer JM. Cysteine-containing fusion tag for site-specific conjugation of therapeutic and imaging agents to targeting proteins. *Methods Mol Biol*. 2008;494:275–94.
81. Moharir A, Peck SH, Budden T, Lee SY. The role of N-glycosylation in folding, trafficking, and functionality of lysosomal protein CLN5. *PLoS One*. 2013;8(9):e74299.
82. Tokhtaeva E, Mareninova OA, Gukovskaya AS, Vagin O. Analysis of N- and O-Glycosylation of Lysosomal Glycoproteins. *Methods Mol Biol*. 2017;1594:35–42.
83. Liebminger E, Hüttner S, Vavra U, Fischl R, Schoberer J, Grass J, et al. Class I alpha-mannosidases are required for N-glycan processing and root development in *Arabidopsis thaliana*. *Plant Cell*. 2009 Dec;21(12):3850–67.
84. Watanabe I, Zhu J, Recio-Pinto E, Thornhill WB. Glycosylation affects the protein stability and cell surface expression of Kv1.4 but Not Kv1.1 potassium channels. *A*

- pore region determinant dictates the effect of glycosylation on trafficking. *J Biol Chem.* 2004 Mar 5;279(10):8879–85.
85. Escribá P v, Busquets X, Inokuchi J ichi, Balogh G, Török Z, Horváth I, et al. Membrane lipid therapy: Modulation of the cell membrane composition and structure as a molecular base for drug discovery and new disease treatment. *Prog Lipid Res.* 2015 Jul;59:38–53.
  86. van Meer G, Voelker DR, Feigenson GW. Membrane lipids: where they are and how they behave. *Nat Rev Mol Cell Biol.* 2008 Feb;9(2):112–24.
  87. Nasr ML, Baptista D, Strauss M, Sun ZYJ, Grigoriu S, Huser S, et al. Covalently circularized nanodiscs for studying membrane proteins and viral entry. *Nat Methods.* 2017;14(1):49–52.

## **7 Appendix**

### **1. Publication in Science : Structural basis for the docking of mTORC1 on the lysosomal surface**

## 2. Cloning Primers

---

### RagA

5' sequencing primer : TTCTGTTCCAGGGGCCCAACACCGCTATGAAAAAAAAAAG

3' sequencing primer : AGCAGCCGGATCTCATCAGCGCATCAGCAGGCTG

### RagC

5' sequencing primer : TCTGTTCCAGGGGCCCTCACTGCAATACGGTGCTG

3' sequencing primer : CAGCCGGATCTCATCAGATTGCATTACGCGGGG

### Ragulator

5' sequencing primer : GAAAACCTGTACTTTCAGGGCGGGTGCTGCTACAG

3' sequencing primer : GCCCTGAAAGTACAGGTTTTCCACCAGAAGACAGATCCG

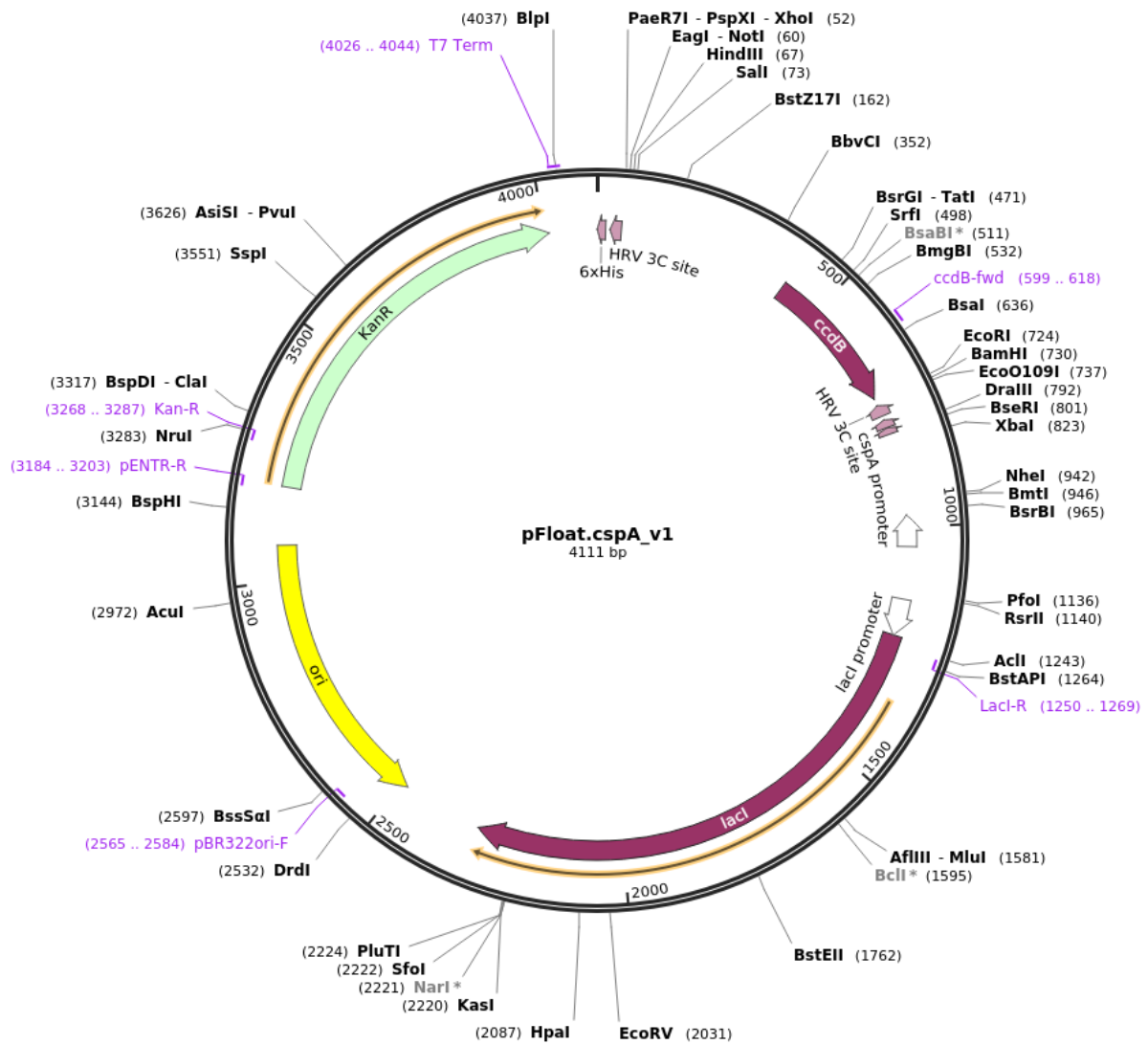
### NW11

5' sequencing primer : AGAGGAGAATACTAGATGAGCACCTTTAGCAAAGTGC

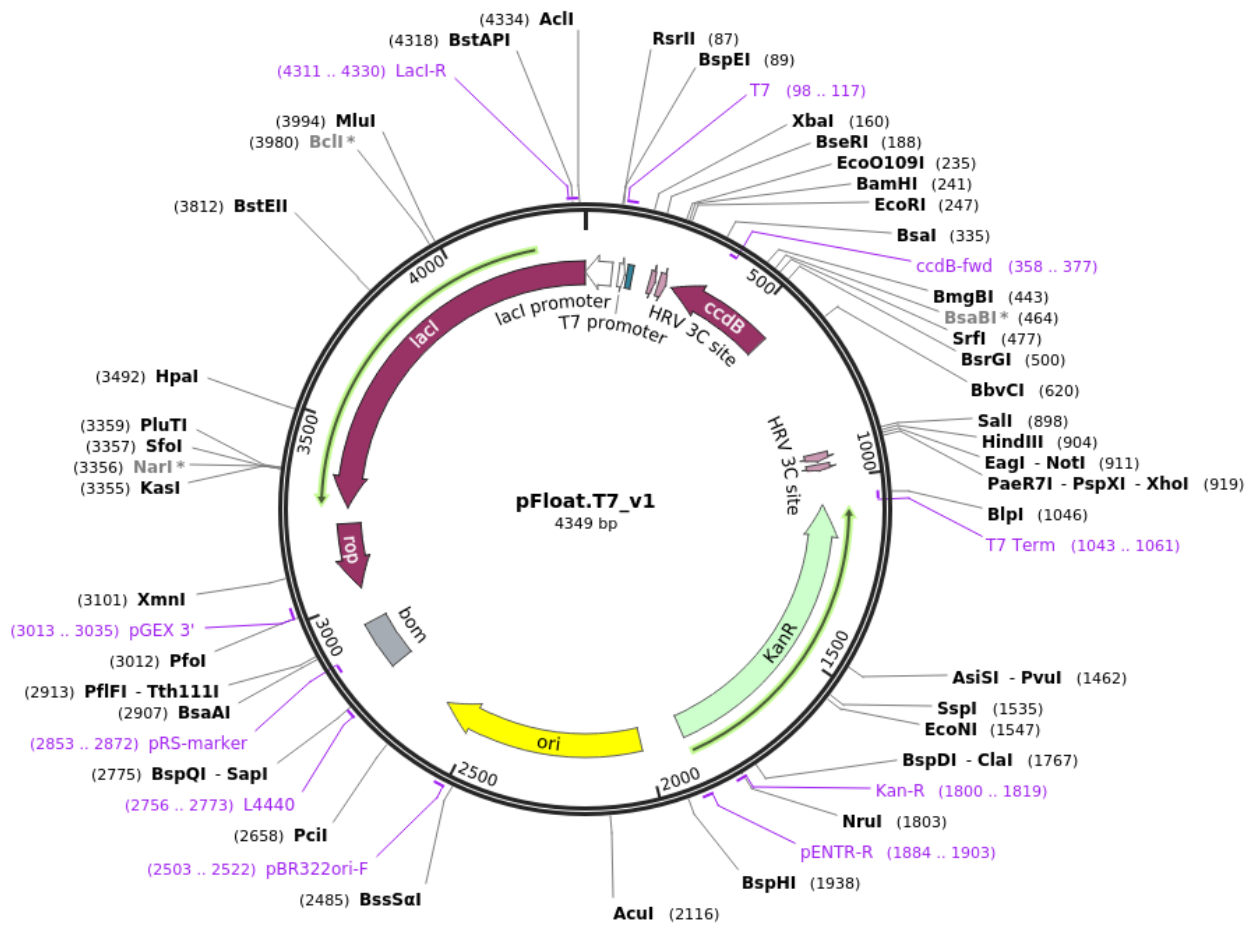
3' sequencing primer : GAAGATGTCGTTTCAGACCGCACCCACCCTGGGTGTTTCAGTTTTTTGG

### 3. Cloning vectors

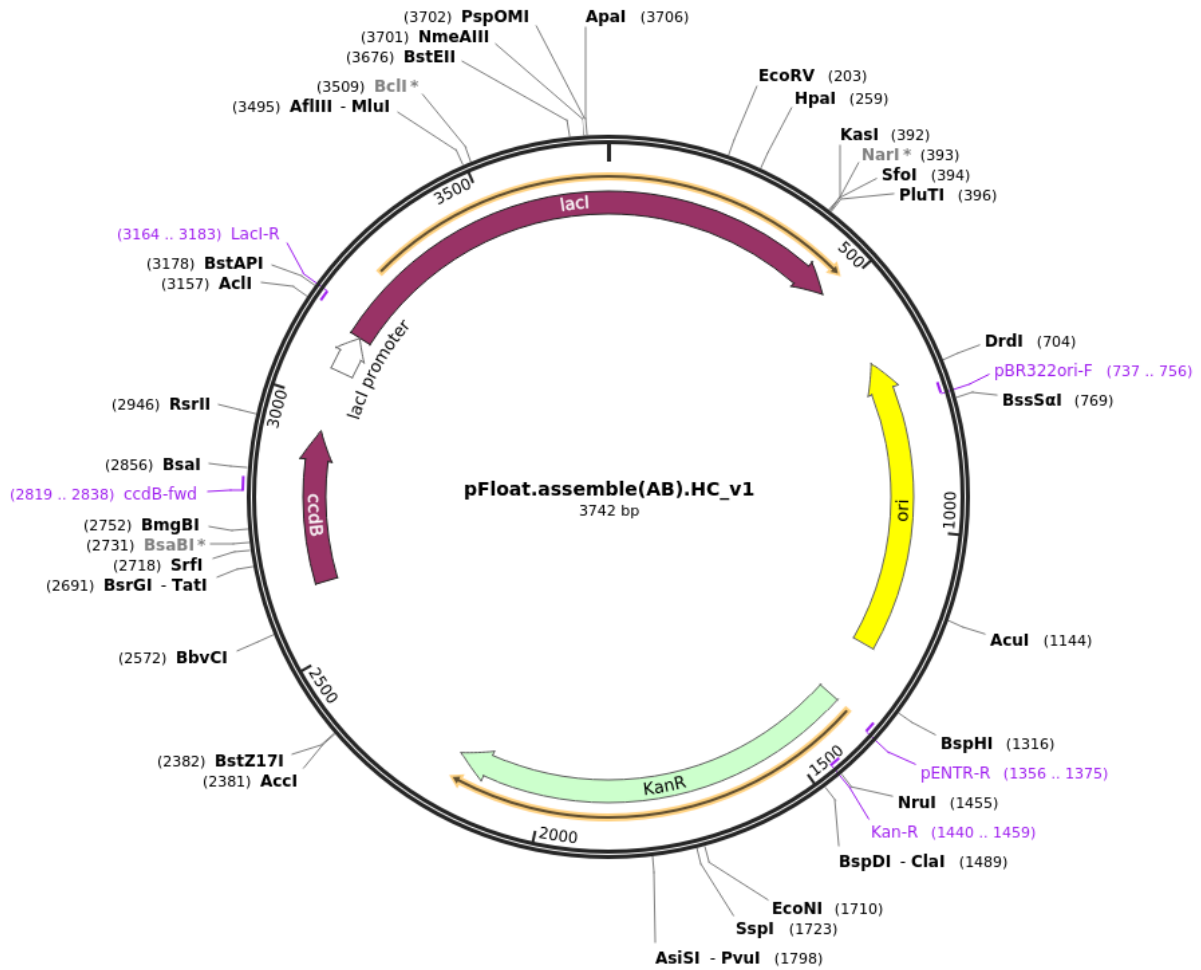
## Cloning vector Rag-GTPases



# Cloning vector NW11



# Cloning vector Ragulator



# 4. Miniprep Kit Protocol

Quick-Start Protocol

February 2015

## QIAprep® Spin Miniprep Kit

The QIAprep Spin Miniprep Kit (cat. nos. 27104 and 27106) can be stored at room temperature (15–25°C) for up to 12 months.

For more information, please refer to the most recent version of the *QIAprep Miniprep Handbook*, which can be found at: [www.qiagen.com/handbooks](http://www.qiagen.com/handbooks).

For technical assistance, please call toll-free 00800-22-44-6000, or find regional phone numbers at: [www.qiagen.com/contact](http://www.qiagen.com/contact).

### Notes before starting

- Optional: Add LyseBlue reagent to Buffer P1 at a ratio of 1 to 1000.
  - Add the provided RNase A solution to Buffer P1, mix and store at 2–8°C.
  - Add ethanol (96–100%) to Buffer PE before use (see bottle label for volume).
  - All centrifugation steps are carried out at 13,000 rpm (~17,900  $\times g$ ) in a conventional table-top microcentrifuge.
1. Pellet 1–5 ml bacterial overnight culture by centrifugation at >8000 rpm (6800  $\times g$ ) for 3 min at room temperature (15–25°C).
  2. Resuspend pelleted bacterial cells in 250  $\mu$ l Buffer P1 and transfer to a microcentrifuge tube.
  3. Add 250  $\mu$ l Buffer P2 and mix thoroughly by inverting the tube 4–6 times until the solution becomes clear. Do not allow the lysis reaction to proceed for more than 5 min. If using LyseBlue reagent, the solution will turn blue.

Sample to Insight



4. Add 350  $\mu$ l Buffer N3 and mix immediately and thoroughly by inverting the tube 4–6 times. If using LyseBlue reagent, the solution will turn colorless.
5. Centrifuge for 10 min at 13,000 rpm (~17,900  $\times g$ ) in a table-top microcentrifuge.
6. Apply 800  $\mu$ l supernatant from step 5 to the QIAprep 2.0 spin column by pipetting. For centrifuge processing, follow the instructions marked with a triangle (▲). For vacuum manifold processing, follow the instructions marked with a circle (●). ▲ Centrifuge for 30–60 s and discard the flow-through, or ● apply vacuum to the manifold to draw the solution through the QIAprep 2.0 spin column and switch off the vacuum source.
7. Recommended: Wash the QIAprep 2.0 spin column by adding 0.5 ml Buffer PB. ▲ Centrifuge for 30–60 s and discard the flow-through, or ● apply vacuum to the manifold to draw the solution through the QIAprep 2.0 spin column and switch off the vacuum source.  
**Note:** This step is only required when using endA+ strains or other bacteria strains with high nuclease activity or carbohydrate content.
8. Wash the QIAprep 2.0 spin column by adding 0.75 ml Buffer PE. ▲ Centrifuge for 30–60 s and discard the flow-through, or ● apply vacuum to the manifold to draw the solution through the QIAprep 2.0 spin column and switch off the vacuum source. Transfer the QIAprep 2.0 spin column to the collection tube.
9. Centrifuge for 1 min to remove residual wash buffer.
10. Place the QIAprep 2.0 column in a clean 1.5 ml microcentrifuge tube. To elute DNA, add 50  $\mu$ l Buffer EB (10 mM TrisCl, pH 8.5) or water to the center of the QIAprep 2.0 spin column, let stand for 1 min, and centrifuge for 1 min.
11. If the extracted DNA is to be analyzed on a gel, add 1 volume of Loading Dye to 5 volumes of purified DNA. Mix the solution by pipetting up and down before loading the gel.

For up-to-date licensing information and product-specific disclaimers, see the respective QIAGEN kit handbook or user manual. Trademarks: QIAGEN®, QIAprep® (QIAGEN Group). 1091289 02/2015 HB.1921-001 © 2015 QIAGEN, all rights reserved.

A few adjustments were made to the protocol :

- 350  $\mu$ L of P1 and P2 was used for steps 2 and 3
- 450  $\mu$ L of N3 was used for step 4
- For step 5, the tubes were centrifuged for 30 minutes at 21 000 g to make sure to get rid of all the debris.

## 5. Buffers

### Lysis Buffer A (Rag GTPases)

---

- ❖ 50 mM HEPES pH 7
- ❖ 100 mM NaCl
- ❖ 2 mM MgCl<sub>2</sub>
- ❖ 1 mM TCEP
- ❖ 0.5 mM PMSF
- ❖ protease inhibitors (EDTA-free, Roche, half dose) - **1 tablet per 100 mL**
- ❖ Lysozyme - a tip of spatula (human recombinant, expressed in rice, 100,000 units/mg protein, Sigma Aldrich)
- ❖ Universal Nuclease (Pierce) - 0.01 µL per mL of lysate
- ❖ 0.15 mM GTP
- ❖ 0.1% Tween20

### Lysis Buffer B (Ragulator)

---

- ❖ 50 mM HEPES pH 7.5
- ❖ 100 mM NaCl
- ❖ 1 mM TCEP
- ❖ 0.5 mM AEBSF
- ❖ protease inhibitors (EDTA-free, Roche, half dose) - **1 tablet per 100 mL**
- ❖ Lysozyme - a tip of spatula (human recombinant, expressed in rice, 100,000 units/mg protein, Sigma Aldrich)
- ❖ Universal Nuclease (Pierce) - 0.02 µL per mL of lysate
- ❖ 0.1% Tween20

### Lysis Buffer C (NW11)

---

- ❖ 50 mM HEPES pH 7
- ❖ 100 mM NaCl
- ❖ 1 mM TCEP
- ❖ 0.5 mM PMSF
- ❖ protease inhibitors (EDTA-free, Roche, half dose) - **1 tablet per 100 mL**
- ❖ Lysozyme - a tip of spatula (human recombinant, expressed in rice, 100,000 units/mg protein) (Sigma Aldrich)
- ❖ Universal Nuclease (Pierce) - 0.01  $\mu$ L per mL of lysate
- ❖ 0.1% Tween20

### Lysis Buffer D (SLC38A9)

---

- ❖ 50 mM HEPES pH 8.0
- ❖ 500 mM NaCl
- ❖ 1 mM TCEP
- ❖ 1 mM PMSF
- ❖ protease inhibitors (EDTA-free, Roche, half dose) - **1 tablet per 100 mL**
- ❖ Lysozyme - a tip of spatula (human recombinant, expressed in rice, 100,000 units/mg protein, Sigma Aldrich)
- ❖ Universal Nuclease (Pierce) - 0.01  $\mu$ L per mL of lysate
- ❖ 10% Glycerol

### Size exclusion (SEC) buffer for the Rag GTPases and Complex reconstitutions

---

- ❖ 25 mM HEPES pH 7.5
- ❖ 100 mM NaCl
- ❖ 0.5 mM  $MgCl_2$
- ❖ 0.5 mM TCEP

### **Ragulator SEC Buffer**

---

- ❖ 25 mM HEPES pH 7.5
- ❖ 100 mM NaCl
- ❖ 0.1 mM AEBSF
- ❖ 0.5 mM TCEP

### **NW11 SEC Buffer**

---

- ❖ 25 mM HEPES pH 7.5
- ❖ 150 mM NaCl
- ❖ 0.5 mM MgCl<sub>2</sub>
- ❖ 1 mM DDM

### **SLC38A9 SEC Buffer**

---

- ❖ 25 mM HEPES pH 8.0
- ❖ 150 mM NaCl
- ❖ 0.04% DDM
- ❖ 0.5 mM TCEP

### **Nanodisc reconstitution SEC Buffer**

---

- ❖ 25 mM HEPES pH 8.0
- ❖ 150 mM NaCl
- ❖ 0.5 mM TCEP

## 6. Hardware and Units

Hardware	Manufacturer
Microcentrifuge 5427 R	Eppendorf
Avanti Centrifuge JXN-26	Beckman Coulter
Ultracentrifuge Optima XE	Beckman Coulter
Äkta Purification System	GE Healthcare
Nanodrop 2000	Thermo fisher

### Units of measurement

g	gram	L	Liter
mg	milligram	mL	milliliter
µg	microgram	µL	microliter
Da	Dalton	nm	nanometer
kDa	Kilo Dalton	mM	millimolar
°C	Degree celcius	µM	micromolar
M	Molar	nmol	nanomol
V	Volt		